

Nonlinear Mathematical and Numerical Modeling of the Effect of Temperature on Membrane Pore Size

A thesis by

Yuhang Qiao

Master of Science in Mechanical Engineering

Submitted to the Faculty of Graduate Studies
in Partial Fulfillment of the Requirements for the
Master's Degree in Mechanical Engineering

Thunder Bay, Ontario

September 2022

Abstract

Due to the growth of the global population, water stress has risen sharply. However, water stress in high latitudes is not only due to population growth but also to low local temperatures. Numerous studies have shown that temperature affects the pore size of membranes, becoming larger at higher temperatures and smaller at lower temperatures. Since the average low temperature at high latitudes is usually below 10°C, the effect of low temperature on the membrane can reduce water flow and thus reduce the effectiveness of the membrane. In this paper, the effect of temperature change on the membrane is mainly studied using the nonlinear thermoelastic model. In the model, an axisymmetric large mechanical deformation as well a large temperature change is considered. Traction-free mechanical boundary conditions and convective thermal boundary conditions were used in the study. The finite difference method is used to solve the nonlinear system of equations. The proposed model is validated by comparison with limited published experimental results. Differences between the model and the published results were analyzed by comparing the MATLAB and experimental results. The effects of the mechanical and thermal properties of the material on the membrane under increasing temperature changes were investigated. The modeling results are in reasonably good agreement with the experimental results.

Keywords: Membrane, Pore size, Temperature, Thermoelasticity, Modeling

Acknowledgements

I am most grateful to my thesis supervisor Dr. H. Bai and co-supervisor Dr. B. Liao, who have provided unlimited guidance and dedication. Their constant encouragement led me to complete my dissertation research during the COVID-19 pandemic. They taught me how to conduct research as clearly as possible, and it was a great honour to work and study with them. At the same time, I would like to express my gratitude to Dr. M. Liu & Dr. L. Cui, very grateful to the two professors for their time and valuable suggestions on my research. And also, thanks to Dr. B. Liao's team, whose research has allowed me to obtain valuable experimental data.

Special thanks go to Mr. Walter Turek, Process Engineer at the Bare Point Drinking Water Membrane Filtration Plant, for his guidance, support, and help in this study. Financial support from NSERC, City of Thunder Bay, and Lakehead University is greatly appreciated.

Finally, I would like to thank all the people who have supported me during the pandemic, especially my parents, whose unconditional support and care have become my strength and helped me complete my thesis.

Yuhang Qiao

Lakehead University

September 2022

Table of Contents

List of Tables.....	1
List of Figures	2
List of Abbreviations.....	4
1. Introduction.....	5
1.1 Global population change	6
1.2 Global water shortage	7
1.3 Temperature in high latitudes	8
1.4 Upgrade water treatment system.....	9
1.5 Classification of membranes	11
1.6 Paragraph summary.....	12
2. Literature review.....	13
2.1 Factors affecting membrane	13
2.1.1 Membrane fouling	13
2.1.2 Membrane pore size	17
2.2 Mathematical models.....	21
2.2.1 Existing model.....	21
2.2.2 Relevant specific models	24
3. Methodology.....	31
3.1 Nonlinear mathematical model.....	31
3.2 Simulation using MATLAB.....	35
3.3 Experiment	35
4. Numerical Results and Analysis	37
4.1 Finite difference (FD) method	38
4.2 Convergence test.....	41
4.3 Model verification	42
4.3.1 Compare with the published results ^[25]	42
4.3.2 Parametric study.....	45
4.3.3 Compare with experimental results from the group.....	47
4.4 Comparing with linear elasticity model.....	54
4.5 Relationship between temperature and pore size change	56
5. Conclusions.....	57

6. Contributions and Improvements	59
6.1 Contribution	59
6.2 Improvements	59
Reference	60
Appendix 1. Average Temperatures in High Latitudes Countries	64
Appendix 2. Pseudo Code and Stopping Criteria.....	65
Appendix 3. Jacobian Matrix.....	67
Appendix 4. F2i and F3i	73

List of Tables

Table 1. 2022 Population Changes (Friday, January 21, 2022) ^[5]	6
Table 2. The effect of pH value on various membranes.....	15
Table 3. Fouling rate and median pore size by two temperatures ^[24]	16
Table 4. The effect of temperature on membrane pore size	18
Table 5. Literature material value.....	42
Table 6. Compare the results with the literature	43
Table 7. Thermal conductivity of different types of PTFE ^[48]	43
Table 8. Experiment results	48
Table 9. Simulation temperature (simulate by experiment inner diameter expansion) at each time.....	49
Table 10. Use temperature at different times to calculate b value	49
Table 11. PVDF physical quantities	51
Table 12. Time to reach steady state under different E	52
Table 13. Time to reach steady state for different inner radii	53

List of Figures

Fig.1. World population and projection to 2100 (Billions) ^[4]	6
Fig.2. Distribution map of water-scarce countries ^[7]	7
Fig.3. Average main cities temperature in Canada (Other countries figure are shown in Appendix 1) ^[8]	8
Fig.4. Old-fashioned water treatment system flow chart ^[9]	9
Fig.5. Flow chart of new water treatment system ^[9]	10
Fig.6. Classification of membranes ^[13]	11
Fig.7. Classification of natural organic matter ^[14]	14
Fig.8. Relationship of membrane temperature and pore size ^[27]	18
Fig.9. The pore size change on a heating stage at 80°C over an 80 minute period ^[25]	19
Fig.10. Flux of reverse osmosis membrane as a function of temperature ^[30]	20
Fig.11. Model structure ^[10]	21
Fig.12. Temperature of the membrane (based on average <i>b</i> value) and Δ Diameter/diameter ^[25]	25
Fig.13. <i>b</i> values ^[25]	25
Fig.14. Cross section of hydrogel ^[38]	27
Fig.15. Membrane Mechanical Structure ^[39]	28
Fig.16. Membrane cross section	32
Fig.17. Image processed by ImageJ	36
Fig.18. Finite difference diagram (two virtual points)	38
Fig.19. Time and expansion in long time step (10s)	41
Fig.20. Inner radius expansion of PTFE membrane	42
Fig.21. The relationship between the thermal conductivity of PVDF and temperature ^[49]	44
Fig.22. Relationship between temperature and inner diameter expansion	44
Fig.23. Inner diameter expansion with different α	45
Fig.24. Time with different α	46
Fig.25. Time reach steady state with different h	47
Fig.26. Time reach steady state with different E	47
Fig.27. Experiment result (normalized inner radius expansion with time)	48
Fig.28. Simulation temperature change (simulate by experiment inner diameter expansion and using the literature ^[25] method) at each time	49

Fig.29. Temperature as function of time (calculated by average b value)	50
Fig.30. Comparison with temperature as function of time (calculate by b value) and experiment inner diameter expansion (The blue line is experiment inner diameter expansion; the orange line is temperature as function of time)	50
Fig.31. Normalized inner radius expansion as function of time	51
Fig.32. Comparison with nonlinear model result of normalized inner radius expansion and experiment result of normalized inner radius expansion from the group	53
Fig.33. Normalized inner radius expansion and time to reach steady state (n=0)	54
Fig.34. Normalized inner radius expansion and time to reach steady state (n=1)	55
Fig.35. Comparison with n=0 and n=1 (by using increasing E value)	55
Fig.36. The normalized inner diameter expansion value variation with temperature (n=0)	56
Fig.37. The normalized inner diameter expansion value variation with temperature (n=1)	56

List of Abbreviations

Abbreviations	Meaning
PDA	Photometric Dispersion Analyzer
PACL	Poly Aluminum Chloride
PTFE	Polytetrafluoroethylene
PVDF	Polyvinylidene Fluoride
UF	Ultrafiltration Membranes
RCOO-	Carboxylate
RCOOH	Carboxylic acid
GE	A membrane, MWCO molecular weight cut-off 1 kDa
GH	A membrane, MWCO molecular weight cut-off 2.5 kDa
GK	A membrane, MWCO molecular weight cut-off 3.5 kDa
C_E, C_p	Specific Heat Capacity (J/(kg·K))
ρ	Density (kg/m ³)
E	Elastic Modulus (N/m ²)
σ	Poisson's Ratio
k	Thermal Conductivity (W/(m·K))
r_i	Inner radius (m)
r_N	Outer radius (m)
T_{ini}, T_{ref}	Initial Temperature (k)
α	Thermal Expansion Coefficient (m/(m·K))
b	The Reciprocal of the Time Constant (/s)
hh	Heat Transfer Coefficient (W/(m ² ·K))
u	Normalized Inner Radius Expansion
$\varepsilon_r, \varepsilon_\theta$	Strain
m	Temperature Nonlinear Coefficient
n	Deformation Nonlinear Coefficient
v	Speed (m/s)

1. Introduction

Water is the source of life, clean drinking water is one top priority in people's daily life because 80% of the human body is water. However, the shortage of water resources is the biggest challenge faced by the human society. From the statistics by the WWF organization, more than 1 billion people worldwide live in water-scarce environments, and countless people die every year due to lack of water ^[1]. Even with the limited water resource accessible and useable for human beings, it is often polluted by wastewater generated by human activities and industrialization. How to solve the water shortage problem has become a common problem for people all over the world.

For over a century, scientists and engineers have put great efforts to develop highly efficient, robust, and low costs of technologies for drinking water treatment. Therefore, traditional water treatment technology can supply good quality of drinking water. ^[2] However, traditional water purification in water treatment plants requires multiple steps, which is complicated and inefficient. If problems are encountered, multi-link inspections are required. Not the same as a traditional water purification system, a membrane filtration system has the advantages of simple operation, low energy cost, low chemical usage, and superior quality of produced drinking water. Therefore, the use of new water treatment membranes is one of the best ways to solve the low work efficiency of water plants.

Although membrane technologies have been used for water treatment systems globally. Due to low temperatures, the seasonal and geographical region temperature changes result in significant challenges for membrane technologies for drinking water treatment, especially in cold regions, like Scandinavia countries, Canada, Russia, and north of China. There has evidence that the cold temperature of raw water has a deteriorated impact on the performance of membrane and membrane fouling in drinking water treatment ^[3]. Thus, the development of a fundamental understanding, such as mathematical modelling, of the impact of temperature (cold and warm temperature) on membrane structure (pore sizes) is of significant industrial significance. The overall goal of this study is to develop mathematical models and numerical modeling to

simulate and predict the impact of cold and warm temperatures on the membrane structure (pore size) in water treatment.

Specific objectives include:

1. To develop mathematical models to model the thermal response of polymeric membranes pore sizes under cold and warm water environments;
2. To model the impact of temperature change on membrane pore sizes; and
3. To verify the accuracy of mathematical models in predicting the thermal response of membrane pore sizes to cold and warm temperature treatment using literature and experimental data.

1.1 Global population change

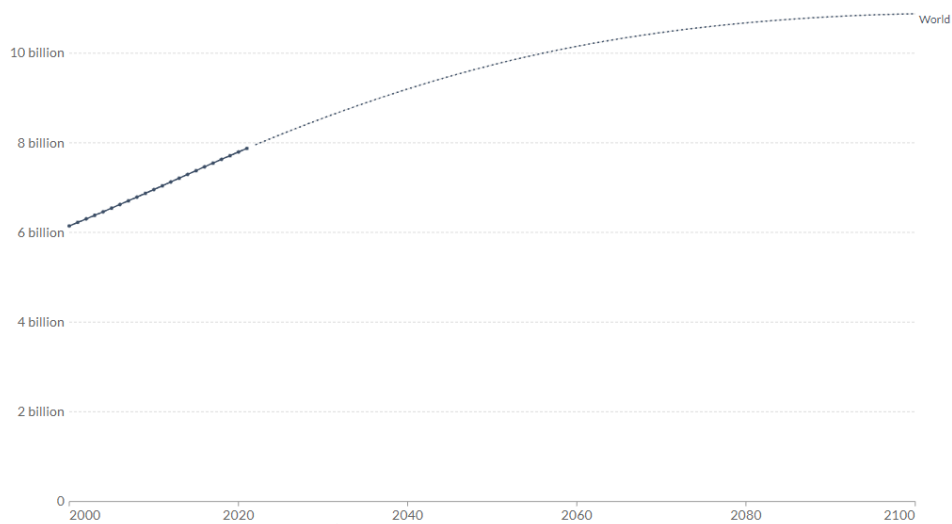


Fig.1 World population and projection to 2100 (Billions) ^[4]

As shown in Figure 1, the growth trend of the global population was from 6 billion in 2000 to almost 8 billion in 2022 and is projected to reach 11 billion by 2100.^[4]

Table 1 2022 Population Changes (Friday, January 21, 2022) ^[5]

Category	Value
Current World Population	7,921,918,216
Births this year	8,033,084
Births today	357,135
Deaths this year	3,372,481

In 2022, the global population has reached 7.9 billion, and such a high population will decrease the total amount of water per capita. Although water resources are renewable resources, the rapid increase in population and the rapid increase in drinking water demand has slowed down the regeneration of water resources. Population rises, food production will rise, and water consumption will increase exponentially.

According to the BBC, “Global water demand is projected to increase by 55% from 2000 to 2050. Agriculture accounts for 70% of global freshwater use, while food production will increase by 69% by 2035 to feed a growing population. On the other hand, the energy-water used to cool the power station will also increase by more than 20%. In other words, there will be another big freshwater crisis soon.” [6]

1.2 Global water shortage

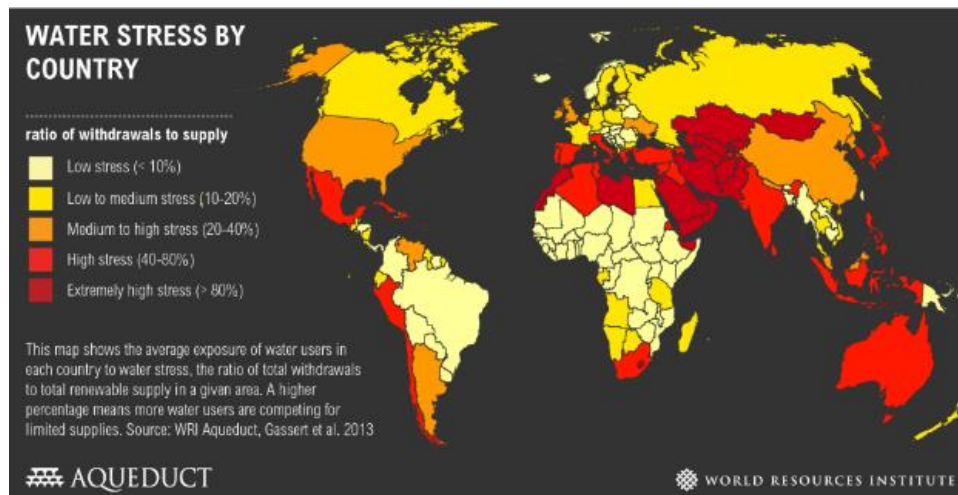


Fig.2 Distribution map of water-scarce countries [7]

As shown in Figure 2, red and dark red are places with extreme water shortage, orange is moderate water shortage, and yellow is moderate to low water shortage.[7] As

shown in the graph, more than 50% of countries have water problems.^[7] Not only in the middle east but also some mid-latitude countries such as Australia, water stress has been a significant challenge. The United States and China are also having moderate to high water stress. Both Northern Europe and Canada have low to moderate water stress. The cause of water shortage in mid-latitude countries is largely caused by the uneven distribution of water resources. It is the temperature that causes water stress at high latitudes.

1.2 Temperature in high latitudes

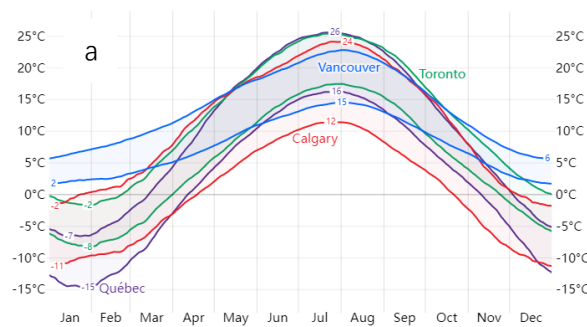


Fig.3 Average main cities temperature in Canada (Other country's figure is shown in Appendix 1) ^[8]

Figure 3 shows the annual temperature distribution map of 5 countries and their main cities. Figure 3-a is the annual average temperature map of various regions in Canada. From Figure 3, it is clear that the temperature in these countries is below zero for half of the time and below 10°C for almost 80% of the time. The well-known normal temperature generally refers to 20 °C, and the same is true for the normal temperature of water treatment. 10°C is already a low-temperature state, and it is difficult to treat water at temperatures of 0°C and below because water will freeze at 0°C. Low-temperature conditions will cause great difficulty in water treatment and will also

greatly affect the process of water treatment. Therefore, improving the water treatment efficiency and decreasing the frequency of repairing and error rate in the treatment process are urgent issues.

1.4 Upgrade water treatment system

The temperature has a huge impact on water treatment, especially in older water treatment systems. The old-fashioned system includes a total of 7 steps from the water inlet to the outlet, namely: 1. Influent; 2. Flocculation; 3. Settlement; 4. Disinfection; 5. Adsorption; 6. Filtration; 7. Supply to users.^[9]

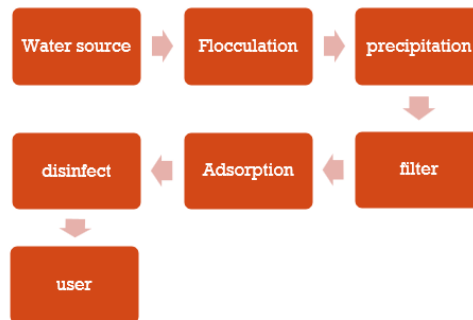


Fig.4 Old-fashioned water treatment system flow chart ^[9]

In this traditional system, many steps will be affected by a large range of temperatures. Take flocculation as an example, the decrease in temperature will lead to deflocculation and decreased flocculation. ^[10]

Fitzpatrick et al. (2004) ^[11] studied the effect of flocculation at different temperatures and used a photometric dispersion analyzer (PDA) to evaluate the flocculation effect. Different flocculants were tested separately, including alum, ferric sulfate and poly aluminum chloride (PACL). The results of the study confirmed that all flocculants had a low flocculation efficiency at a lower temperature, and the formation of flocs was slower. ^[11]

If the flocculation is formed slowly, the settling time is delayed, and the flocculation efficiency is not ideal, which may lead to the failure of settling and filtration. And sedimentation and filtration are also affected by temperature, so optimizing the water treatment method is a good way to avoid risks. [11, 12]



Fig.5 Flow chart of new water treatment system [9]

Some studies confirmed that all flocculants had a low flocculation efficiency at a lower temperature, and the formation of flocs was slower. [11-12]

The new water treatment system as shown in Fig.5, can effectively improve water treatment efficiency. The process of the new system has a total of 4 steps: 1. Water inlet; 2. Filtration; 3. Disinfection; and 4. Supply to users.^[9] It is straightforward, from the original seven steps to the current four steps, that omitting the process of flocculation, adsorption, and sedimentation, has effectively reduced the influence of temperature on these three steps.^[9] If something goes wrong, it is only a matter of filtration. Solving the problems in the filtration will allow a better maintenance of the new system without having to go to check one step by one step.

The problems in the new water treatment system are basically on the membrane. The membrane problem can be better solved by understanding the effect of temperature

on the membrane structure and performance. Therefore, this thesis focuses on the relationship between membrane structure and temperature.

1.5 Classification of membranes

To understand the relationship between membranes and temperature, we need to understand the types of membranes. Currently, membranes used for water treatment are divided into four categories, as shown in Figure 6.

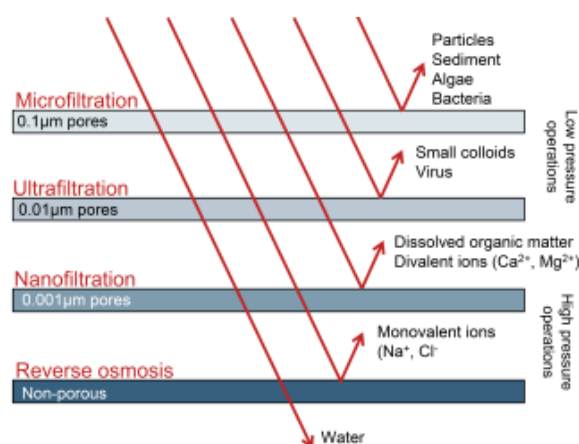


Fig.6 Classification of membranes ^[13]

These four types are divided according to the membrane's pore size, which is: 1. Microfiltration, 2. Ultrafiltration, 3. Nanofiltration, 4. Reverse osmosis.^[13] The first two types of membranes are generally used in low-pressure operations and can filter out the macromolecule; the latter two membranes, generally used in high-pressure operations, can filter out a portion of the ions.^[13]

The filtration efficiency of nanofiltration will be better than the first two membranes, because the pore size of nanofiltration is smaller, it is even more affected by temperature.

In addition to using membranes with smaller pore sizes, new water treatment systems will also use better filtration methods.

1.6 Paragraph summary

Global drinking water stress has gradually evolved from a local problem to a global problem, due to rapid population growth and industrialization. High latitudes have more freshwater reserves. However, there is not much fresh water in low latitudes. The temperature in high latitudes is generally low, and the water treatment system will be significantly affected by the low temperature. Therefore, improving the water treatment system is an excellent way to reduce the pressure of drinking water production effectively. Because of the cumbersome and complicated steps of the old water treatment system, it has been upgraded and changed to a new type of membrane systems for water treatment in a number of regions including cold regions, which can improve the water treatment efficiency and decrease the probability of problems occurred in the water treatment processes.

2. Literature review

2.1 Factors affecting membrane

2.1.1 Membrane fouling

Membrane fouling which decreases membrane performance is a significant bottleneck of membrane process technology. Membrane fouling can cause water treatment flux declines and affect the quality of water produced.^[14]

The factors that cause membrane fouling are diverse. The main types of foulants are inorganic and organic matters. There have a lot of reasons for membrane fouling, the first is the membrane material problem, and the second is the natural causes. These include ^[14]:

- 1) Natural Organic Matter (NOM);
- 2) pH;
- 3) Hydrophilicity/hydrophobicity of the foulants and membranes;
- 4) Ionic strength;
- 5) Temperature.

(1) Natural organic matter (NOM)

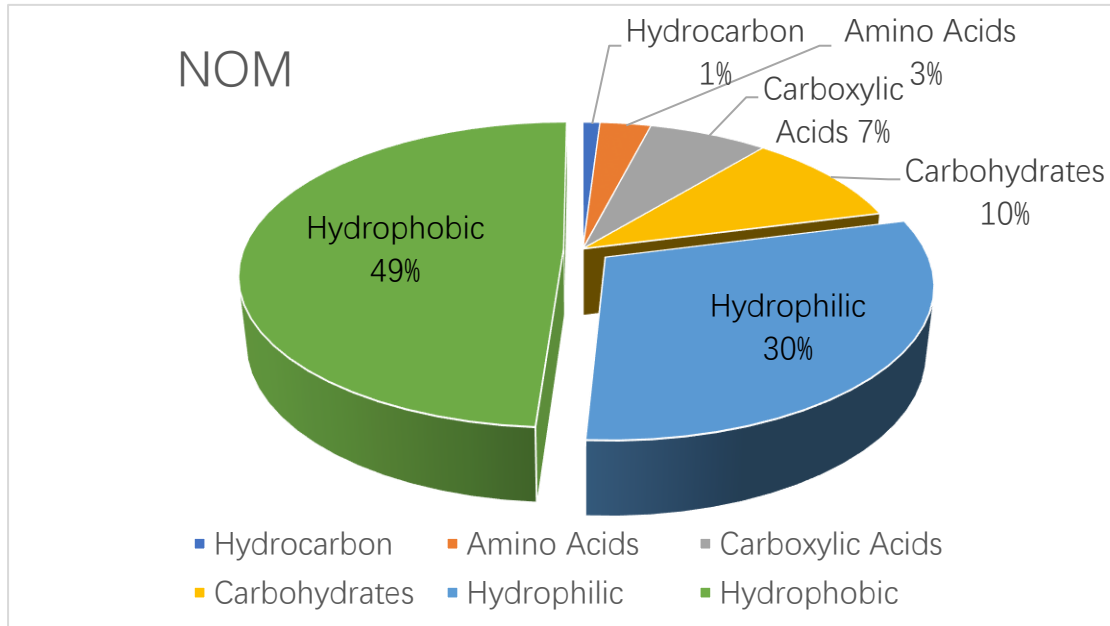


Fig.7 Classification of natural organic matter ^[14]

NOM is a part of the aquatic environment and contains polymers like carbohydrates, proteins, humic acids etc.^[15] Drinking water sources generally contain NOM ^[15]. NOM negatively affects many steps in the water treatment process and is one of the main factors leading to membrane fouling, because ultrafiltration membranes cannot remove NOM effectively. ^[16] NOM pollution is not only related to chemical related mature fields but also to physical fields. ^[17]

(2) PH value

PH value reflects the pH value of the liquid and is an essential factor affecting the degree of membrane fouling. Due to the different pH values of the liquids being processed, the degree of membrane fouling is also different. At higher pH values, the flow of water is greater, and membrane fouling is less than at lower pH values. Table 2 summarizes some studies on the effect of pH on the membrane.

Table 2 The effect of pH value on various membranes

Membrane materials	PH	Effect	References
NF membrane	4,8	Decreased water flow	Hong and Elimelech, 1997 ^[17]
UF membrane	11	Increased electrons to reduce membrane fouling	Lin et al., 2001 ^[18]
NF/UF membrane	High	Impurity sedimentation to reduce membrane fouling	Schafer, 2001 ^[19]

Hong & Elimelech (1997) ^[17] found that the water flux decreased at pH 4 and 8 and there was more intensive fouling at lower pH value.

Lin's experiments found that NOM had more carboxyl groups (RCOO⁻) at higher pH ^[18], and they became protonated carboxyl groups (RCOOH) at lower pH, which resulted in a decrease in charge of the humus and increased membrane fouling. ^[18]

Schafer et al. (2001) ^[19] found that a high pH value was conducive to calcite precipitation, and calcite could adsorb organic molecules, so calcite adsorbed organic molecules to the surface and precipitates, reducing the membrane fouling by organic molecules.

(3) Hydrophilicity/Hydrophobicity of foulants and membranes

Bogati et al. (2012) ^[20] found that regardless of membrane type, hydrophilic compounds such as carbohydrates are the leading cause of physically irreversible fouling of membranes. Moreover, at the same time, hydrophobic compounds (such as

humic substances) are adsorbed in the membrane matrix through interactions and act as carbohydrate binders to stick carbohydrates to the membrane, enhancing membrane fouling significantly.^[20] Therefore, the hydrophobic membrane, such as the PVDF membrane, is more likely to adsorb hydrophobic compounds such as humic substances.

(4) Ionic strength

The ionic strength affects the degree of membrane fouling. Hong and Elimilech (1997)^[17] found that membrane fouling becomes more severe as the ion concentration increases. Due to the increase in ionic strength, a large number of Na⁺ ions enter the solution, which leads to a sharp drop in the level of negatively-charged molecules, which in turn causes the adsorption of soluble substances on the membrane.^[17]

Lin et al. (2001)^[18] found that an increase in ionic strength results in the adsorption of pollutant molecules to the membrane surface to form membrane fouling.^[18]

(5) Temperature

There are many effects caused by changes in temperature, which will affect the pH value^[21,22] and natural organic matter^[23] mentioned above. Thus, the effect of temperature is enormous. The most intuitive effect is the pore size of the membrane.^[24]

Table 3 Fouling rate and median pore size by two temperatures^[24]

Temperature	Fouling rate kPa/day	Median pore size (μm)
10°C	0.65	26
20°C	0.45	48

It is evident from Table 3 that the median pore size at 20 °C is 48 μm, which is 22 μm larger than that at 10 °C, which is the direct effect of temperature on membrane fouling.^[24]

To summarize this part, five factors, including 1.) Natural organic matter; 2.) PH value; 3.) Hydrophilicity and hydrophobicity; 4.) Ionic strength; 5.) Temperature.), will affect the performance of the membrane. The first three will affect the physical properties of the substances in the water, resulting in membrane fouling and thus a smaller pore size of the membrane. In addition, the ionic strength changes the chemical properties of the substances in the water, causes membrane fouling, and lead the membrane's pore size to decrease by building foulants in membrane pores.

Temperature is a significant factor because temperature not only affects the molecular size of the substances in the solution, causing membrane fouling. Moreover, it can also affect the pore size of membrane so that directly affect the filtration of the membrane.

2.1.2 Membrane pore size

The pore size of the membrane determines the filtration performance of membrane and also how the membrane is used. Membrane pore size is the most crucial factor affecting filtration. The type of membrane materials and the fabrication processes and conditions of membrane will basically control the pore size. Each material has different physical properties, including porosity and pore size.

However, the results show that temperature can affect the membrane pore size significantly, which affects the membrane performance.

Table 4 The effect of temperature on membrane pore size

Membrane Type	Temperature Effects	Reference
PTFE	As the temperature increases, the pore size gradually increases. ^[25]	A.J. Hughes, et al., (2020)
Lot M38 & Lot M39	The pore size range from 6 to 60 μ m. ^[26]	Rodolfo (2010)

Table 4 shows that temperature affects the pore size of the PTFE and LotM38 and M39 membranes. The higher the temperature, the larger the pore size.

Rizki et al. (2020)^[27] investigated the effect of temperature on three different filtration membranes through experiments and modelling. Studies showed that as the temperature increases, the pore size of the membrane would expand while reducing its hydraulic resistance. Furthermore, the relationship between membrane pore size and the temperature is shown in Figure 8.

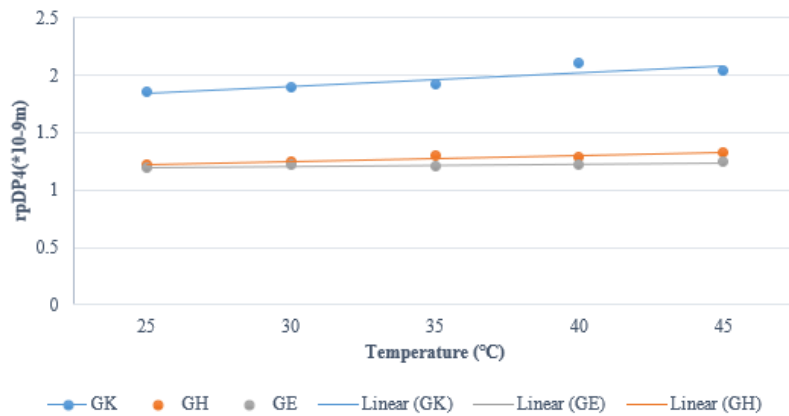


Fig.8 Relationship of membrane temperature and pore size^[27]

(1) High-temperature environment

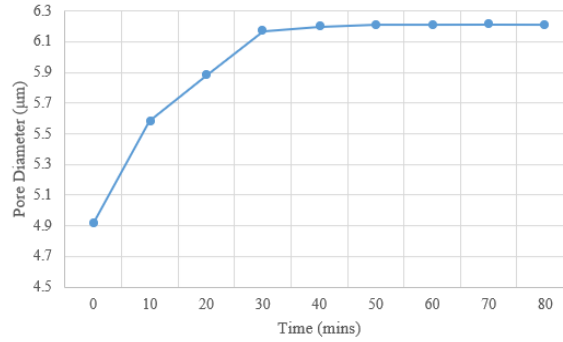


Fig.9 The pore size change on a heating stage at 80°C over an 80-minute period [25]

Hughes et al. (2020) [25] experimentally studied the effect of temperature on membrane pore size, as shown in Figure 9. The membrane was placed at an ambient temperature of 80°C for 80 minutes of heating treatment. The pore size increases sharply in the first 30 minutes, and then increases slowly in the last 50 minutes. [25] From an initial diameter of 4.94 µm, it reached a steady state of 6.28 µm. A difference of 1.34 µm is equivalent to an increase of 27%, which is a significant increase. [25]

(2) Low temperature

The impact of a low temperature state on the membrane is even more significant. Since the environmental temperature is around 20°C, the performance test of the membrane is generally carried out at room temperature. Therefore, the effect of low temperature on membrane would not be examined in detail in the membrane fabrication process.

Fan et al. (2016) [28] found that the cold-water temperatures lead to decreased membrane permeability and shrinkage of membrane pore size. Therefore, the water temperature will affect the filtration efficiency of the ultrafiltration membrane. The

membrane-specific flux at 11.0 °C is about 88% of that at 14.4 °C. Thus, the lower the water temperature, the smaller the membrane-specific flux of the ultrafiltration system.

[28]

Shen et al. (2013) [29] found that the temperature dramatically influenced the membrane flux, and when the temperature dropped to below 5 degrees Celsius, the flux decay rate was increased by 30%.

Figure 10 shows the flux of reverse osmosis membrane as a function of temperature.

[30]

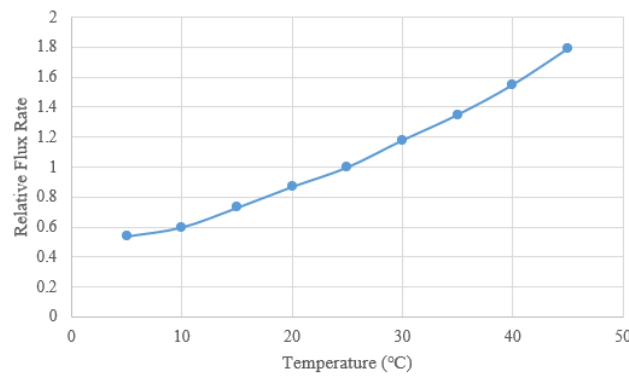


Fig.10 Flux of reverse osmosis membrane as a function of temperature [30]

It is clear that the relative flux of the reverse osmosis membrane is about 0.86 at room temperature (20°C), but the relative flux is only 0.53 when the water temperature is 5°C, as compared with the reference water temperature of 25°C. [30] Therefore, a low temperature significantly reduces the flux of filtration and dramatically increases the time required for water treatment or needs more membrane surface areas. The water flux is related to the membrane pore size so that the temperature affects membrane performance by influencing the pore size and water viscosity directly.

Temperature can directly affect the membrane pore size, and the membrane water treatment efficiency. Developing mathematical models to study the impact of temperature on membrane pore size is of significant industrial significance. With the mathematical models in place, the performance of membrane can be optimized and predicted under different temperatures.

2.2 Mathematical models

2.2.1 Existing model

There are many models studying the impact of temperatures on membrane structure and performance. For example, some models study their impacts on membrane pore size, while other models describe their impacts on membrane permeability. Furthermore, the research angles are also different, some are from the energy perspective, the molecular perspective, and the chemical perspective and so on.

Marriott et al. (2003) ^[10] modeled the membrane assembly from the perspective of mass, momentum, and energy balance, and the model structure is shown in Figure 11.

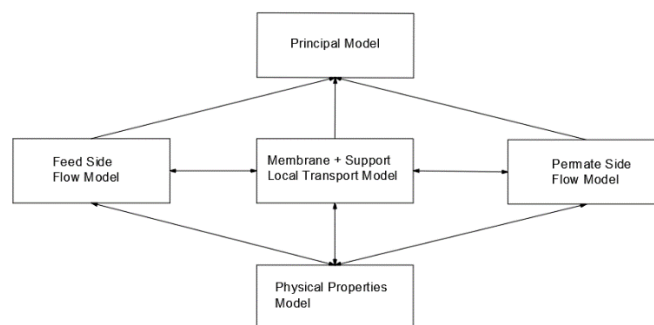


Fig.11 Model structure^[10]

From the energy perspective, the authors studied the effect of the feed side, membrane structure, and permeate side on the membrane performance and then correlated them to the performance and achieved the final overall model.^[10]

Mohammad et al. (2002)^[31] proposed a modified Donnan-steric-pore model, based on the Nernst-Planck equation, combining charge and steric effects. The model uses three parameters to simulate the performance of the membrane: 1.) Effective pore size r_p 2.) Membrane thickness to porosity ratio $\Delta x/A_k$ 3.) Charge density X_d . This model can be used for evaluating the retention capacity and flux behavior of NF membranes in binary solutions and mixtures preliminarily.^[31]

Bowen et al. (2002)^[32] investigated a model of the repulsion of uncharged solutes. These include the effect of chemical potential on pressure and the change in solvent viscosity with pore size. This change does not affect rejection for pores of a single size, but if considering pore size distribution, it becomes crucial for overall membrane rejection. The modeling results are in good agreement with the experimental data, which confirms that this continuum model can be used to describe the repulsion of uncharged solutes in nanofiltration membranes.

Mukhopadhyay et al. (2014)^[33], after considering various models, proposed a model in Hilbert space that can be well applied to various general materials.^[33] The model is based on the coupled dynamic thermoelasticity theory with a basic Green-Lindsay-type model.

Mukhopadhyay et al. (2015)^[34] established a two-temperature model in Hilbert space. The model is based on irreversible thermodynamics, coupled with

thermoelasticity, and discusses the adaptability of the equations, avoiding the square root of unbounded operators.

Zhang et al. (2021) ^[35] proposed a new thermoelasticity model for significant temperature changes in an isotropic material. To describe the thermoelastic behaviour of solids when experiencing significant temperature changes, the authors proposed a new finite element model coupled with thermos-elasticity and performs experimental verification.^[35] The authors believe that with the same conditions of small deformation, the significant temperature change is compared with the small change.^[35] A significant temperature change can be seen as a small deformation increases the specific heat. The model discusses the problem of the coupled thermoelastic model under the framework of small deformation. Significant temperature change establishes a finite element model and uses the backward difference method to calculate the model.^[35] Using 304 steel as the experimental sample for the experimental test, the experimental results and numerical calculation results showed that both the axial strain and the tangential strain will increase exponentially with the temperature increase. Moreover, under the condition of significant temperature change, the solid near the boundary will change more violently, which increases with the magnitude of temperature change. ^[35]

Ehsan et al. (2014) ^[36] studied a model, based on generalized thermos-elasticity theory and non-Fourier heat conduction, and established an equation model for coupled thermoelastic control of Timoshenko microbeams.^[36] The model can capture microscale structure size effects. In this paper, the simply supported microbeam is taken

as a case study, and the micro-beam coupling thermo-elastic equation of the normalized form of the dimensionless thermal moment is obtained. [36]

Siddhartha (2019) [37] used micropolar thermos-elasticity theory to study the plane waves in linear propagate in isotropic porous materials.[37] In order to calculate the phase velocity and attenuation coefficient, the modified aluminum-epoxy resin composite material was taken as an example to solve, and a variety of situations were considered. Furthermore, the elasticity and other conditions were calculated and compared. Finally, the relationship between phase velocity and frequency, attenuation coefficient and frequency were obtained. [37]

2.2.2 Relevant specific models

(1) Model 1 (thermodynamic model) [25]

Hughes et al. (2020) [25] proposed a model which describes the relationship between temperature and time, derived from energy balance.

$$\frac{T(t) - T_{\infty}}{T_i - T_{\infty}} = e^{-bt} \quad (2.1)$$

where

T is the temperature; K

$T(t)$ is the temperature at the current time; K

T_{∞} is the environmental temperature; K

T_i is the initial temperature, K

b is a physical constant reflecting the relationship between time and temperature needs to be calculated according to the measured pore size at different times, 1/s.

Figure 12 shows the relationship between the growth value of the diameter and the time (blue line). Sampling and analysis are carried out every 10 minutes, and the red curve is drawn from 10-80 minutes.^[25] Using the relationship between $\Delta D/D$ and time, perform the calculation as follows,

$$\frac{\Delta D/D(t) - \Delta D/D_{\infty}}{\Delta D/D_t - \Delta D/D_{\infty}} = e^{-bt} \quad [25] \quad (2.2)$$

Calculating b every 10 minutes, and the result is shown in Figure 12.

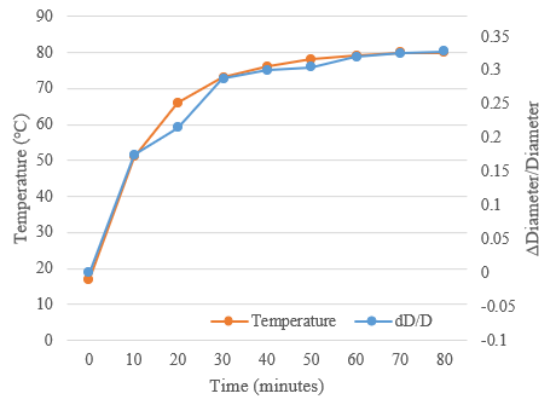


Fig.12 Temperature of the membrane (based on average b value) and Δ Diameter/diameter ^[25]

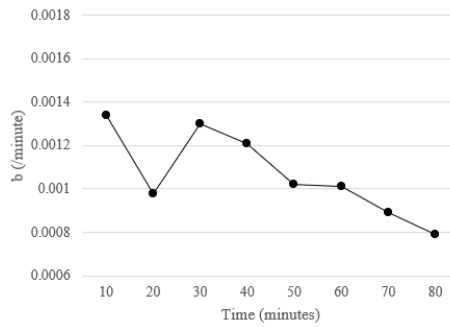


Fig.13 b value ^[25]

As shown in Figure 13, the b value has a significant fluctuation at 20 minutes, which is also an essential reason for the downward movement of the point at 20 minutes in Figure 12.

The temperature change with time (orange line) in Figure 12 was obtained by using equation (2.1) and average b value for the first 40 minutes.

(2) Model 2 (elasticity model) ^[38]

Chatterjee et al. (2003) ^[38] developed a mathematical model for hydraulic membranes. The model considers chemical reactions due to concentration gradients and electrostatic potentials, de-crosslinking, etc., and physical reactions to changes in hydrogel modulus. ^[38] This model needs to, first, calculate the potential and determine the relationship between φ_{new} and φ_{old} , and then calculate the distribution of substance concentration over time, according to the chemical reaction equation. As the concentration changes, the modulus of the hydrogel will also change, and the modulus of the hydrogel is related to the fluid volume fraction, so the modulus of the hydrogel can be calculated by the Equation (2.3).^[38] Finally, the mechanical model of the hydrogel is calculated according to Equation (2.4).

$$E = E_0 \left(1 - 2([C])/([C] + [B])\right) \left(\frac{1}{H+1}\right)^{1/3} \quad [38] \quad (2.3)$$

where

E is the elastic modulus;

E_0 is the initial modulus;

[B], [C] are the concentrations of B ions and C ions;

H is the hydration of the hydrogel.

$$\nabla \cdot \sigma = 0 \quad (2.4)$$

σ is stress tensor.

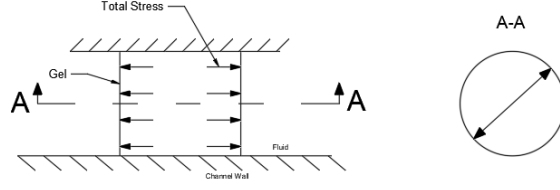


Fig.14 Cross section of hydrogel [38]

The model (equation (2.4)) is a two-dimensional axisymmetric model. Therefore it can be simplified as:

$$\frac{\partial \sigma_r}{\partial r} + \frac{\sigma_r - \sigma_t}{r} = 0 \quad (2.5)$$

$$\sigma_r = \frac{E}{(1 + \nu)(1 - 2\nu)} \left[(1 - \nu) \frac{\partial u}{\partial r} + \nu \frac{u}{r} \right] - (P_{osmotic} + \sigma_{residual}) \quad (2.6)$$

$$\sigma_t = \frac{E}{(1 + \nu)(1 - 2\nu)} \left[(1 - \nu) \frac{u}{r} + \nu \frac{\partial u}{\partial r} \right] - (P_{osmotic} + \sigma_{residual}) \quad (2.7)$$

where r is the radius, σ_r and σ_t are solved using Equations (2.6) and (2.7), respectively

σ_r and σ_t are radial stress and tangential stress, respectively.

E is elastic modulus; ν is the Poisson's ratio;

$P_{osmotic}$ is the osmotic pressure, which is related to ion concentration, calculated by using Equation (2.8);

$\sigma_{residual}$ is the residual stress, which is related to the initial modulus of the hydrogel and initial hydration, calculated using Equation (2.9).

$$P_{osmotic} = RT \sum_{k=1}^N (c_k - c_k^0) \quad (2.8)$$

R is the universal gas constant;

T is the temperature;

c_k is the concentration of the k^{th} chemical;

c_k^0 is the c_k in the outside the hydrogel.

$$\sigma_{residual} = E_0 \left(\frac{1}{H_0 + 1} \right)^{1/3} H_0 \quad (2.9)$$

E_0 is the initial modulus of the hydrogel;

H_0 is the initial hydration of the hydrogel.

(3) Model 3 (thermoelastic model) ^[39]

Park et al. (2016) ^[39] designed a reversible membrane structure with pores that can be changed by the temperature variation. This membrane structure will open and close the pores according to the increase and decrease of the ambient temperature and control the ventilation rate of the membrane pores. This membrane structure is mainly modelled according to the relevant heat transfer formulas and structural mechanics. According to the model simulation, the pores can be fully opened at 40°C, and the porosity is 100%; at 20°C, the pores are closed, and the porosity is 0%. The model takes only 20 minutes to grow from 20°C to 40°C and can be bent with a maximum bending angle of 45°. ^[39]

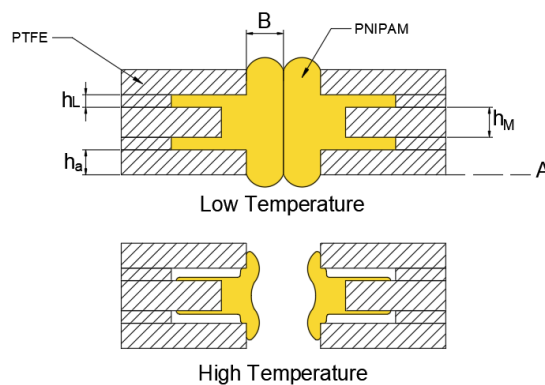


Fig.15 Membrane Mechanical Structure ^[39]

As shown in Figure 15, the structure of the membrane is an axisymmetric structure, which can be considered as a combination of three kinds of plates with circular holes

and an inner elastic material after decomposition. Using a plate with a height of h_a as the upper and lower surfaces, a plate with a height of h_m in the middle, and two plates with a height of h_L is used to connect the three plates. The middle of the pore is filled with an elastic material, which could shrink and expand according to the decrease and increase of temperature, respectively. From the Figure 15, it is clear that when the temperature is low, the pore with B is closed and is in a closed state. However, at high temperatures, the pore size opens and becomes open.^[39]

According to the material's properties, the authors believe that the combination of thermodynamic and elastic mechanics equations (equation (2.10)) can allow the model to have a better description of the relationship between the opening and closing of membrane pores and temperature. Equation (2.10) is as follow:^[39]

$$\rho C_p \frac{\partial T}{\partial t} + T_0 \frac{\partial S_{elast}}{\partial t} - \nabla \cdot (k \nabla T) = 0^{[39]} \quad (2.10)$$

where,

ρ is the density;

C_p is specific heat capacity;

T is the temperature;

t is time.

S_{elast} is the elastic strain, calculate by using Equation (2.11).

$$S_{elast} = \alpha_{vec} \cdot (\sigma_x + \sigma_y + \sigma_z)^{[39]} \quad (2.11)$$

α_{vec} is the thermal expansion coefficient, σ_x , σ_y , σ_z are the normal stress in three directions.

In summary, three existing mathematical models have been developed to describe the relationship between temperature, stress, pore size and time. Each model has its limitations.

To the best of the author's knowledge, solving thermoelastic problems on the condition of significant temperature changes has not been well discussed.^[35] Furthermore, modelling microporous media such as membranes using thermoelasticity is even more limited. Moreover, according to the published research, the pore sizes usually have a large change in diameter. It will result in a large normal strain.

Therefore, the membrane pores are modelled by using theory of thermoelasticity. The large deformation and the large temperature change will be introduced into the model as well in this study. The aim is to obtain a nonlinear mathematical model for studying the change in pore size of the membranes under temperature change. To the best of my knowledge, there is no such model reported in the literature.

3. Methodology

Considering the large pore size change and large temperature change, a coupled nonlinear thermoelastic model is proposed in this chapter. First, the mathematical model is developed. Second, the solution method is outlined. Third, an experimental result is briefly introduced.

The pore as well as its size is randomly distributed in the membrane, for example, see below Figure 17. Furthermore, the distance among pores is relatively large when compared with their sizes. As the first step, in this study a single pore model will be proposed and studied. The interaction among pores is neglected in the current model. In the proposed model, the membrane with a single pore is modelled as a hollowed thin disk, as shown in Figure 16.

In the current study, the membrane is treated as an isotropic material. The deformation of the membrane will be assumed to be axisymmetric.

3.1 Nonlinear mathematical model

As shown in Figure 16, inner radius is r_1 and outer radius is r_n . Outer radius is determined by experiment and published paper which typical value is around 10 times of inner radius.

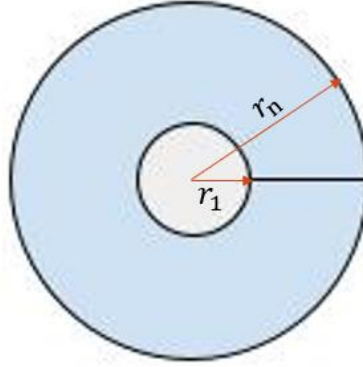


Fig.16 Membrane cross section

Consider a thin disk emerged into static fluid with a constant temperature. The deformation of the membrane is axisymmetric, a state of plane stress is used in the study.

The displacement field and the membrane temperature are assumed to be

$$\begin{cases} u_r = u(r, t) \\ u_\theta = 0 \\ T = TT(r, t) - T_{ref} \end{cases} \quad (3.1)$$

where,

u_r is displacement in the radial direction;

u_θ is the displacement in the circumferential direction;

$TT(r, t)$ is the temperature of the membrane;

T_{ref} is the reference temperature;

T is the relative temperature of membrane.

For axisymmetric deformation, the normal strain components are given as follow

$$\begin{cases} \varepsilon_r = \frac{\partial u}{\partial r} + \frac{n}{2} \left(\frac{\partial u}{\partial r} \right)^2 \\ \varepsilon_\theta = \frac{u}{r} + \frac{n}{2} \left(\frac{u}{r} \right)^2 \end{cases} \quad (3.2)$$

where,

ε_r is the normal strain in radial direction;

ε_θ is the normal strain in circumferential direction.

Here $n = 0$ is the linear model (small strains) and $n = 1$ is the nonlinear model (large strains).

Dynamic equation of the membrane in the radial direction is given by

$$\frac{\partial \sigma_r}{\partial r} + \frac{\sigma_r - \sigma_\theta}{r} = \rho \frac{\partial^2 u}{\partial t^2} \quad (3.3)$$

where,

σ_r is the stress in radial direction;

σ_θ is the stress in circumferential direction.

Hooke's law for plane stress is given by

$$\begin{cases} \sigma_r = \frac{E}{1-\nu^2} (\varepsilon_r + \nu \varepsilon_\theta) - \frac{1-2\nu}{1-\nu} cT \\ \sigma_\theta = \frac{E}{1-\nu^2} (\nu \varepsilon_r + \varepsilon_\theta) - \frac{1-2\nu}{1-\nu} cT \end{cases} \quad (3.4)$$

where,

E is the elastic module;

ν is Poisson's ratio;

c is specific heat capacity.

Substituting equations (3.2) and (3.4) into the dynamic equation (3.3), we will have

$$\begin{aligned} n\delta_1 \left[\frac{\partial^2 u}{\partial r^2} \frac{\partial u}{\partial r} + \nu \frac{u}{r^2} \frac{\partial u}{\partial r} + \frac{1-\nu}{2r} \left(\frac{\partial u}{\partial r} \right)^2 - \frac{1+\nu}{2r^3} u^2 \right] \\ + \delta_1 \left(\frac{\partial^2 u}{\partial r^2} + \frac{1}{r} \frac{\partial u}{\partial r} - \frac{u}{r^2} \right) - \delta_2 \frac{\partial T}{\partial r} = \frac{\partial^2 u}{\partial t^2} \end{aligned} \quad (3.5)$$

The thermal-coupled mechanical model ^[39] is as follow

$$T_{ref} \left(1 + m \frac{T}{T_{ref}} \right) c\dot{e} + \rho C_e \dot{T} = k \Delta T = k \left(\frac{\partial^2 T}{\partial r^2} + \frac{1}{r} \frac{\partial T}{\partial r} \right) \quad (3.6)$$

where e is volumetric strain defined as follow

$$e = \varepsilon_r + \varepsilon_\theta + \varepsilon_z = \frac{1 - 2\nu}{1 - \nu}(\varepsilon_r + \varepsilon_\theta) + \frac{(1 + \nu)(1 - 2\nu)c}{E(1 - \nu)}T \quad (3.7)$$

Here, $m = 0$ is the linear model (small temperature change) and $m = 1$ is the nonlinear model (large temperature change).

k is the thermal conductivity coefficient

C_e is the specific heat

Substituting equation (3.2) and (3.7) into equation (3.6), we have

$$\begin{aligned} \left[1 + \frac{mT}{T_{ref}} \left(1 - \frac{\rho C_e}{\delta\delta}\right)\right] \frac{\partial T}{\partial t} + \delta_3 \left(1 + \frac{mT}{T_{ref}}\right) \left(\frac{\partial u}{\partial r} \frac{\partial v}{\partial r} + \frac{uv}{r^2}\right) n \\ + \delta_3 \left(1 + \frac{mT}{T_{ref}}\right) \left(\frac{\partial v}{\partial r} + \frac{v}{r}\right) - \delta_4 \left(\frac{\partial^2 T}{\partial r^2} + \frac{1}{r} \frac{\partial T}{\partial r}\right) = 0 \end{aligned} \quad (3.8)$$

where

$$\left\{ \begin{array}{l} \delta_1 = \frac{E}{\rho(1 - \nu^2)} \\ \delta_2 = \frac{c(1 - 2\nu)}{\rho(1 - \nu)} \\ \delta_3 = \frac{T_i c(1 - 2\nu)}{\delta\delta(1 - \nu)} \\ \delta_4 = \frac{k}{\delta\delta} \\ \delta_5 = \frac{c(1 - \nu - 2\nu^2)}{E} \\ \delta\delta = \rho C_e + \frac{T_{ref} c^2(1 - \nu - 2\nu^2)}{E(1 - \nu)} \end{array} \right. \quad (3.9)$$

The mechanical boundary conditions are traction-free which are given as follow:

At $r = r_1$ and $r = r_N$

$$\frac{1 - \nu^2}{E} \sigma_r(r, t) = \frac{1}{2} \left[\left(\frac{\partial u}{\partial r}\right)^2 + \frac{\nu}{r^2} u^2 \right] n + \delta_1 \left(\frac{\partial u}{\partial r} + \frac{\nu u}{r}\right) - \delta_5 T = 0 \quad (3.10)$$

The convection thermal boundary conditions are given by

$$\left\{ \begin{array}{l} -k \frac{\partial T}{\partial r} = h(T - TGV) \quad r = r_1 \\ k \frac{\partial T}{\partial r} = h(T - TGV) \quad r = r_N \end{array} \right. \quad (3.11)$$

where

$$TGV = T_{\infty} - T_{ref}$$

TGV is the total change in temperature

h is the convection heat transfer coefficient

Initial conditions:

$$\text{At } t=0: T = 0, u = 0, v = \frac{du}{dt} = 0.$$

3.2 Simulation using MATLAB

It is convenient to use MATLAB to write matrices and vectors and quickly find the solution, allowing a graphical view of the results and easy testing of the effect of different material constants on the pore size expansion and temperature variation.

This thesis uses MATLAB to solve the nonlinear partial differential equations. Firstly, using the finite difference method to transform the nonlinear partial differential equation into nonlinear algebraic equations, and then the MATLAB code is developed to solve the nonlinear algebraic equations.

The detailed process is presented in chapter 4.

3.3 Experiment

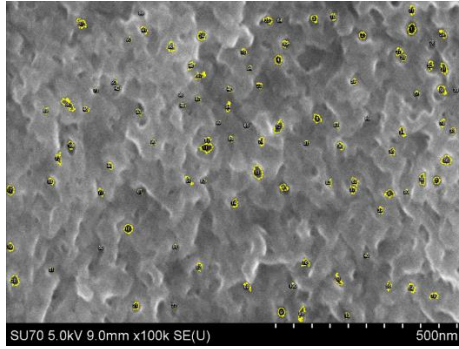


Fig.17 Image processed by ImageJ

Professor Liao's team provided the experimental results as shown in Figure 17. The software ImageJ is used to analyze the images, recording the pore size value at different times.

The experimental results from the literature and a graduate student (Mr. Xu) are used in the thesis to compare the results computed from the proposed nonlinear mathematical model.

4. Numerical Results and Analysis

Numerical solutions will be used to solve the proposed nonlinear system of partial differential equations in Chapter 3.

Many available numerical methods were studied, for example, boundary element method, finite element method, finite difference method and etc. Each method has its own advantages and disadvantages. Boundary element method ^[40, 41] is more suitable for solving linear differential equations because of the requirement of the Green's functions of the system, even it requires less computational resources comparing with the finite element method. Finite element method ^[42, 43] can handle large engineering problems with complex and irregular domains, however, it requires to process large amount of data and not easy to program. Finite difference method ^[44], on the other hand, can directly discretize the domain of the problem and is suitable for regular geometric domains. It is relatively easy to develop the computer program.

Thus, in this chapter, the finite difference method will be employed to solve the nonlinear PDE proposed in Chapter 3. In the study, the MATLAB code was developed first, and the convergence test was studied. Then numerical results from MATLAB were compared with available published results as well the experimental results from Dr. Liao's team. Finally, the parametric study of effect of material properties on the pore size expansion and the time required to reach steady state of the membrane was exploited.

4.1 Finite difference (FD) method

As shown in the Figure18, this line represents the radius, N equally spaced points is used in the discretization, as shown in equation (4.1). Furthermore, when central difference formula is used, two virtual points are presented which are represented by r_0 and r_{N+1} , respectively.

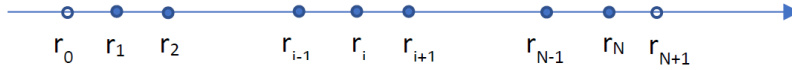


Fig.18 Finite difference diagram (two virtual points)

The radius of each finite difference point is given as follow

$$r_i = r_1 + (i - 1)H, \quad i = 1, 2, 3, \dots, N, \quad H = \frac{r_N - r_1}{N - 1} \quad (4.1)$$

where H is length of each segment.

The first order of the central difference of each variable is given below as

$$\left(\frac{\partial T}{\partial r}\right)_i = \frac{T_{i+1} - T_{i-1}}{2H}, \quad \left(\frac{\partial u}{\partial r}\right)_i = \frac{u_{i+1} - u_{i-1}}{2H}, \quad \left(\frac{\partial v}{\partial r}\right)_i = \frac{v_{i+1} - v_{i-1}}{2H} \quad (4.2)$$

Here T is temperature, u is displacement and v is velocity.

The second order of the central difference the corresponding variables is given below as

$$\left(\frac{\partial^2 T}{\partial r^2}\right)_i = \frac{T_{i+1} - 2T_i + T_{i-1}}{H^2}, \quad \left(\frac{\partial^2 u}{\partial r^2}\right)_i = \frac{u_{i+1} - 2u_i + u_{i-1}}{H^2} \quad (4.3)$$

For the stress boundary conditions, forward and backward FD are used for the inner and outer radii, respectively, to avoid solving a quadratic equation when calculating the virtual node values:

$$\left(\frac{\partial u}{\partial r}\right)_1 = \frac{-3u_1 + 4u_2 - u_3}{2H} \quad (4.4)$$

$$\left(\frac{\partial u}{\partial r}\right)_N = \frac{3u_{N-2} - 4u_{N-1} + u_N}{2H} \quad (4.5)$$

The equations (3.5) and (3.8) can be written as, at node i ,

$$\begin{cases} \frac{\partial u_i}{\partial t} = v_i \\ \frac{\partial v_i}{\partial t} = F2_i(u_{i-1}, u_i, u_{i+1}, T_{i-1}, T_{i+1}) = F2_i \\ B_i \frac{\partial T_i}{\partial t} = F3_i(u_{i-1}, u_i, u_{i+1}, v_{i-1}, v_i, v_{i+1}, T_{i-1}, T_i, T_{i+1}) = F3_i \end{cases} \quad (4.6)$$

where

$$\begin{cases} B_1 = b_1 + 2H\delta_5 d_1 \\ B_i = b_i, \quad i = 1, 2, 3, \dots, N-1 \\ B_N = b_N + 2H\delta_5 d_N \end{cases}$$

$$\begin{cases} d_1 = \left(\frac{u_2 - u_0}{2H} n + 1 \right) \frac{\delta_3}{2H} c_1 \\ d_N = \left(\frac{u_{N+1} - u_{N-1}}{2H} n + 1 \right) \frac{\delta_3}{2H} c_N \end{cases} \quad (4.7)$$

$$\begin{cases} b_i = 1 + m \frac{T_i}{T_{ref}} \delta_6 \\ c_i = 1 + m \frac{T_i}{T_{ref}} \\ \delta_6 = 1 - \frac{\rho C_e}{\delta \delta} \end{cases}$$

The expression of F2i and F3i are given in the Appendix 4.

The Crank-Nicolson method is used to solve the nonlinear system equations. [45]

$$\begin{cases} \left[\frac{\partial u_i}{\partial t} = v_i \right]^{j+\frac{1}{2}} \\ \left[\frac{\partial v_i}{\partial t} = F2_i \right]^{j+\frac{1}{2}} \\ \left[B_i \frac{\partial T_i}{\partial t} = F3_i \right]^{j+\frac{1}{2}} \end{cases} \quad (4.8)$$

$$\begin{cases} \frac{u_i^{j+1} - u_i^j}{\Delta t} = \lambda v_i^{j+1} + (1 - \lambda) v_i^j \\ \frac{v_i^{j+1} - v_i^j}{\Delta t} = \lambda F2_i^{j+1} + (1 - \lambda) F2_i^j \\ B_i^j \frac{v_i^{j+1} - v_i^j}{\Delta t} = \lambda F3_i^{j+1} + (1 - \lambda) F3_i^j \end{cases} \quad (4.9)$$

λ is from 0.5 to 1, because when λ in this range equations are unconditional convergence. Δt is time step.

Here

$$t_j = (j - 1)\Delta t, \quad j = 1, 2, \dots, N \quad (4.10)$$

$$\begin{cases} F2_i^{j+1} = F2_i(u_{i-1}^{j+1}, u_i^{j+1}, u_{i+1}^{j+1}, T_{i-1}^{j+1}, T_{i+1}^{j+1}) \\ F2_i^j = F2_i(u_{i-1}^j, u_i^j, u_{i+1}^j, T_{i-1}^j, T_{i+1}^j) \end{cases} \quad (4.11)$$

$$\begin{cases} F3_i^{j+1} = F3_i(u_{i-1}^{j+1}, u_i^{j+1}, u_{i+1}^{j+1}, v_{i-1}^{j+1}, v_i^{j+1}, v_{i+1}^{j+1}, T_{i-1}^{j+1}, T_i^{j+1}, T_{i+1}^{j+1}) \\ F3_i^j = F3_i(u_{i-1}^j, u_i^j, u_{i+1}^j, v_{i-1}^j, v_i^j, v_{i+1}^j, T_{i-1}^j, T_i^j, T_{i+1}^j) \end{cases}$$

Equations (4.9) are a system of nonlinear equations used to find $u_i^{j+1}, v_i^{j+1}, T_i^{j+1}$

Replacing u_i for u_i^{j+1} , v_i for v_i^{j+1} , T_i for T_i^{j+1} , $u_i^{(1)}$ for u_i^j , $v_i^{(1)}$ for v_i^j , and $T_i^{(1)}$ for

T_i^j , the nonlinear system (4.11) can be re-write as follows

$$\begin{aligned} f1_i &= u_i - \lambda \Delta t v_i - u_i^{(1)} - (1 - \lambda) \Delta t v_i^{(1)} = 0 \\ f2_i &= v_i - \lambda \Delta t F2_i(u_{i-1}, u_i, u_{i+1}, T_{i-1}, T_{i+1}) - v_i^{(1)} \\ &\quad - (1 - \lambda) \Delta t F2_i^{(1)}(u_{i-1}^{(1)}, u_i^{(1)}, u_{i+1}^{(1)}, T_{i-1}^{(1)}, T_{i+1}^{(1)}) \\ f3_i &= B_i^{(1)} T_i - \Delta t F3_i(u_{i-1}, u_i, u_{i+1}, v_{i-1}, v_i, v_{i+1}, T_{i-1}, T_i, T_{i+1}) - B_i^{(1)} T_i^{(1)} \\ &\quad - (1 - \lambda) \Delta t F3_i^{(1)}(u_{i-1}^{(1)}, u_i^{(1)}, u_{i+1}^{(1)}, v_{i-1}^{(1)}, v_i^{(1)}, v_{i+1}^{(1)}, T_{i-1}^{(1)}, T_i^{(1)}, T_{i+1}^{(1)}) \end{aligned} \quad (4.12)$$

$$i = 1, 2, 3, \dots, N$$

Use the Newton method to solve the nonlinear system (4.12):

Using the solution at t_j as the initial guess, ie, $u_i^{(1)}, v_i^{(1)}, T_i^{(1)}$, $i = 1, 2, \dots, N$.

Denote w^- as the initial guess. Denote w as the unknowns u_i, v_i, T_i , ie,

$$w = (u_1, v_1, T_1, u_2, v_2, T_2, \dots, u_i, v_i, T_i, \dots, u_N, v_N, T_N)^T$$

The symbolic writing of equations (4.12) is

$$G(w) = \begin{Bmatrix} f1_1 \\ f2_1 \\ f3_1 \\ \vdots \\ f1_N \\ f2_N \\ f3_N \end{Bmatrix} = 0$$

Calculate the Jacobian of the system G at the initial guess: $J_{pq}(w^-) = \frac{\partial G_p}{\partial w_q}(w^-)$

Solve $J(w^-) \delta w = -G(w^-)$

Find the approximate solution $w = w^- + \delta w$

Update the initial guess by w .

4.2 Convergence test

In the nonlinear model, the influence of the number of segments and time step on the pore size expansion and the time required to reach steady state will be tested first. The outer diameter is determined by the experimental results, which is 10 to 20 times of the inner diameter. In the following calculation, the outer diameter is taken as 10 times of the inner radius.

Through the convergence test (physical quantities are shown in Table 5), it is found that using 10 segments is enough to reach convergence value of inner radius expansion. As the number of segments increases, it can be found that the inner diameter expansion value has almost no changes, but as the number of segments increased, the time required to reach steady state was decreased.

Different time step (0.001 s, 0.01 s, 0.1 s, 1 s, 10 s) are used in the convergence test. The computational time is inversely proportional to the time step. Furthermore, as shown in the Figure 19 there has a fluctuation of inner radius expansion when time step is chosen as 10 s. So, in the following computation, the time step is chosen as 1 s.

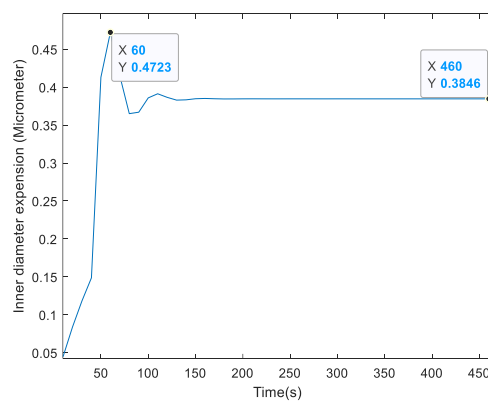


Fig.19 Time and expansion in long time step (10 s)

4.3 Model verification

4.3.1 Compare with the published results ^[25]

The material constant of PTFE shown in Table 5 are used in the simulation. Among those constants, C_E , ρ , the initial temperature, r_1 and r_N are given from the paper, and α is calculated in this thesis. The other constants are found from the website <https://www.matweb.com/> ^[46].

Table 5 Literature material value

Property	value	
Specific Heat Capacity, C_E ^[25]	1090	J/(kg·K)
Density, ρ ^[25]	2200	kg/m ³
Elastic Modulus (25°C), E ^[46]	2.2×10^8	N/m ²
Poisson's Ratio, σ ^[47]	0.05	
Thermal Conductivity, k ^[48]	0.256	W/(m·K)
r_1 ^[25]	2.125×10^{-6}	m
r_N ^[25]	3.16×10^{-5}	m
Reference Temperature, T_{ref} ^[25] (T_{ini})	290.15	K
Thermal Expansion Coefficient, α	0.00316	m/(m·K)
Heat Transfer Coefficient, hh ^[25]	0.56	W/(m ² ·K)

The inner radius expansion of the PTFE membrane from the model are shown in the Figure 20,

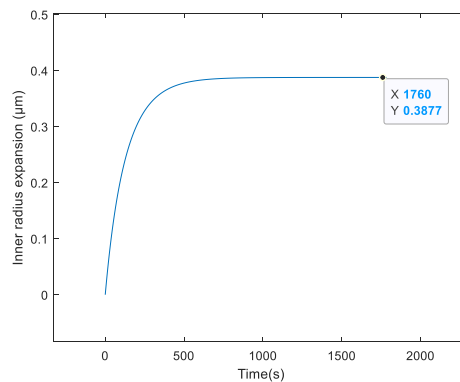


Fig.20 Inner radius expansion of PTFE membrane

Table 6 Compare the results with the paper

	Pape ^[25]	MATLAB Result
Inner radius expansion value (μm)	0.465	0.3877

From the table above it can be seen that there is 16% difference when comparing the numerical result with the result from the paper^[25]. Some possible reasons are discussed in below:

(1) Uncertainty of material constants

Different types of PTFE membranes will have different material constants since different compounds were added during the manufacture process. Furthermore, manufacturers do not disclose material constants and additives because of the confidentiality. Thus, it can be seen from the Table 7 that the lowest thermal conductivity is 193 mW/(m°C), and the highest value is 278 mW/ (m°C).

Table 7 Thermal conductivity of different types of PTFE ^[48]

Sample	k (mWm ⁻¹ °C ⁻¹) at 50°C
Bulk PTFE	259±6
Unsintered PTFE/glass	198±5
Sintered PTFE/glass	222±6
Sintered PTFE/glass+30% Al ^a	271±7

(2) Temperature dependent material constants

For determining material constants, a specific temperature is generally selected for measurement. For example, the thermal conductivity of PTFE in Table 7 is measured at 50 °C.

As shown in Figure 21, PVDF has a different thermal conductivity (k) at different temperatures. In Figure 21, the k of PVDF is about 0.26 at 20 °C, 0.22 at 60 °C, and 0.18 at 100 °C. Due to the change of thermal conductivity with temperature, even if only calculated to 60°C, it still has a gap of 0.04, which is 15% difference of the value at 20 °C, which is already a significant change.

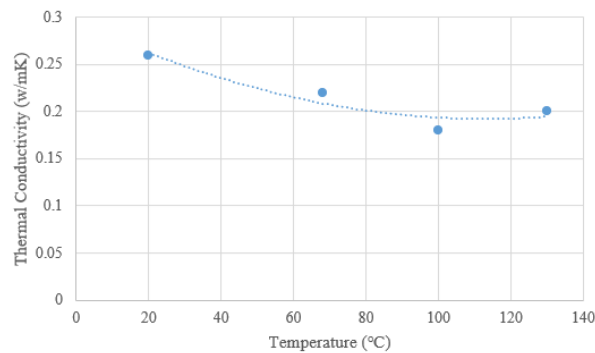


Fig.21 The relationship between the thermal conductivity of PVDF and temperature [49]

This is another reason why there is 16% difference between the simulation and the experiment [25].

In the paper [25], the author assume that inner radius and temperature has a linear relationship. The computational results confirmed that assumption, as shown in the Figure 22 below.

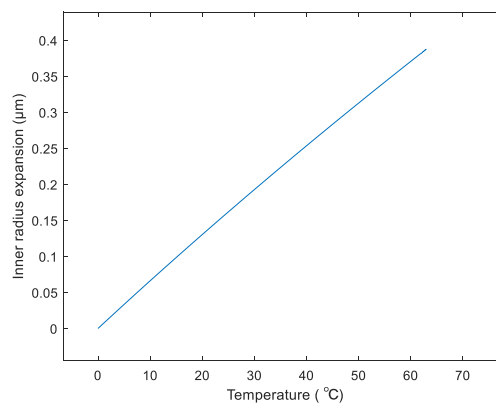


Fig.22 Relationship between temperature and inner diameter expansion

4.3.2 Parametric study

Some material constants affecting the inner radius expansion and the time required to reach steady state are studied in this section.

(1) Thermal expansion coefficient (α)

As shown in the Figure 23, it was found that as α increases, the inner radius expansion will be increased correspondingly. Also, inner radius expansion has an almost linear relationship with α .

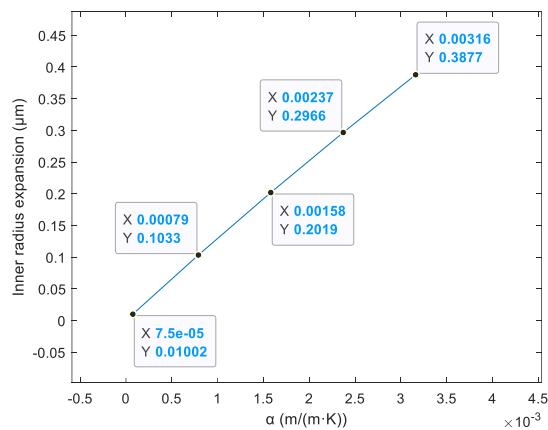


Fig.23 Inner diameter expansion with different α

On the other hand, α growth also leads to an increment of the time required to reach steady state. The results are shown in the Figure 24 below.

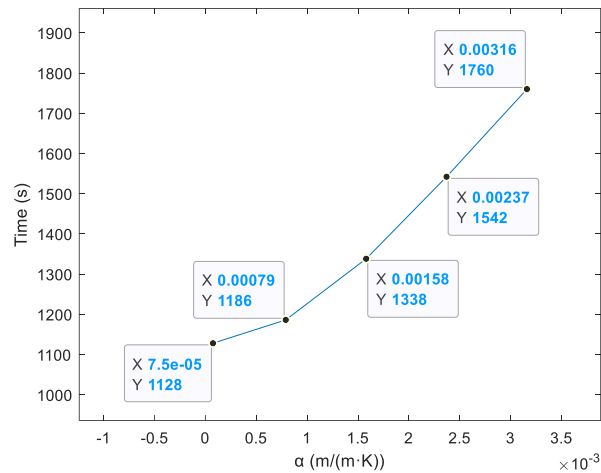


Fig.24 Time with different α

It can be seen that the time required to reach steady state has a nonlinear relationship with α . With the increasing value of α , the time required to reach steady state will be increased as well.

(2) Heat transfer coefficient (hh)

The heat transfer coefficient is calculated in paper ^[25] by using density, specific heat capacity, volume, area and b. hh does not affect the expansion of the inner radius. However, it has a significant impact on the time required to reach steady state. As shown in Figure 25, the larger the value hh, the shorter the time required to reach steady state. Moreover, the Figure 25 shows that it is a nonlinear relationship between the time required to reach steady state and hh.

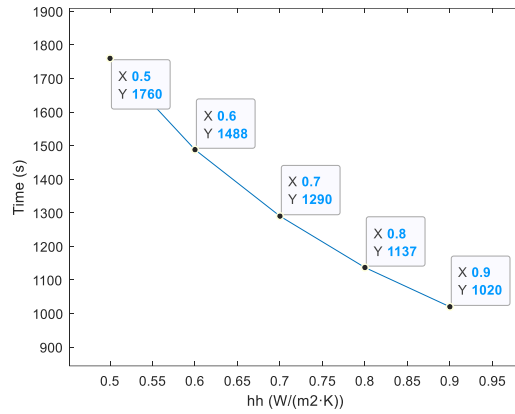


Fig.25 The time required to reach steady state with different hh

(3) Elastic modulus (E)

Through the study on different elastic modulus, it can be found that as elastic modulus increased, the time required to reach steady state also increased. Moreover, as shown in the Figure 26, the time required to reach steady state has an almost linear relationship with the elastic modulus.

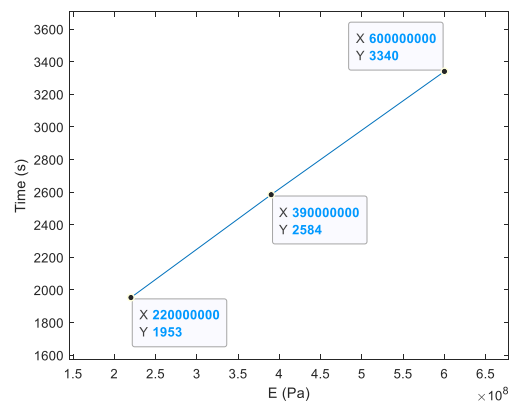


Fig.26 The time required to reach steady state with different E

4.3.3 Compare with experimental results from the group

The experimental data was provided by Professor Liao's group. The experiment temperature is changing from 0.3 °C to 35 °C. The normalized experimental results are shown in the Table 8:

Table 8 Experiment results

Time (minute)	0	30	90	180	300	480	720	1440
Normalized inner radius	1	1.1194	1.1684	1.1465	1.1846	1.2230	1.2406	1.2342

As can be seen from the Table 8, the pore size changes are relatively large.

(1) Calculation of heat transfer coefficient

First, using the method described in the paper [25] to calculate b value. It may be noted that the data at 180 minutes is removed from the computation because it has a sharp drop.

The plot of normalized inner radius expansion is shown in Figure 27.

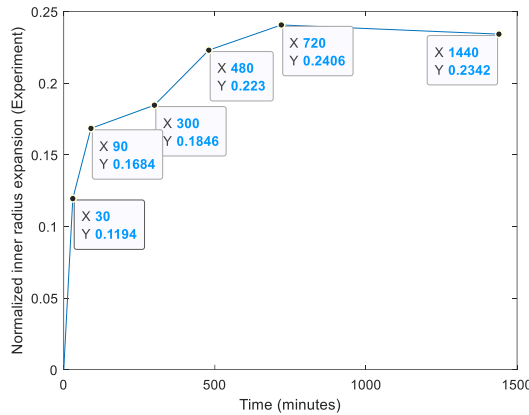


Fig.27 Experiment result (normalized inner radius expansion with time)

Considering that the temperature has a linear relationship with the inner radius expansion, the temperature can be evaluated by using the following equation:

$$T_{(t)} = T_{\infty} + \frac{[\Delta r_{(t)} - \Delta r_{\infty}] * (T_{ini} - T_{\infty})}{\Delta r_{ini} - \Delta r_{\infty}} \quad (4.13)$$

The temperature at each time point is shown in the Table 9.

Time (minutes)	0	30	90	300	480	720	1440
Temperature growth value (°C)	0	17.220	24.287	26.630	32.172	34.700	33.777

This temperature is used to calculate the b value and is given by equation (4.14)

below:

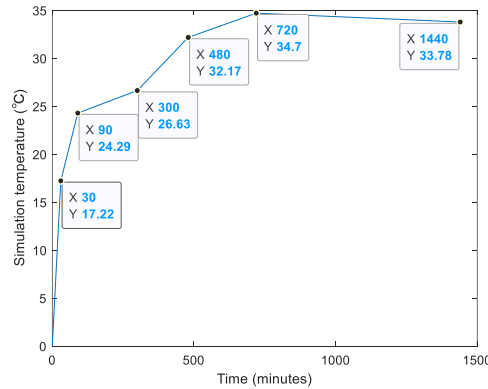


Fig.28 Simulation temperature change (simulate by experiment inner diameter expansion and using the literature [25] method) at each time

$$\frac{(T_{(t)} - T_{\infty})}{(T_{ini} - T_{\infty})} = e^{-bt} \quad (4.14)$$

Table 10 Use temperature on different time to calculate b value

Time	minutes	0	30	90	300	480	720	1440
Temperature	°C	0.3	17.522	23.587	26.93	32.472	35	34.077
b	1/minute		0.022288	0.013062	0.00474	0.005222	0.006553	0.002333

The average value of b is calculated by using the result of which the time is 300,480,720 minutes, which is 0.0054983 (1/min).

Once the value of b is estimated, equation (4.14) will be used to calculate the temperature at different instant of time, and the results are shown in Figure 29 below.

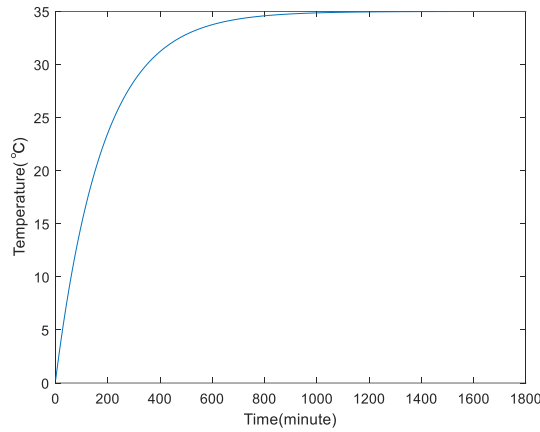


Fig.29 Temperature as function of time (calculated by average b value)

For comparison, the inner radius expansion and the temperature as function of time are shown in Figure 30.

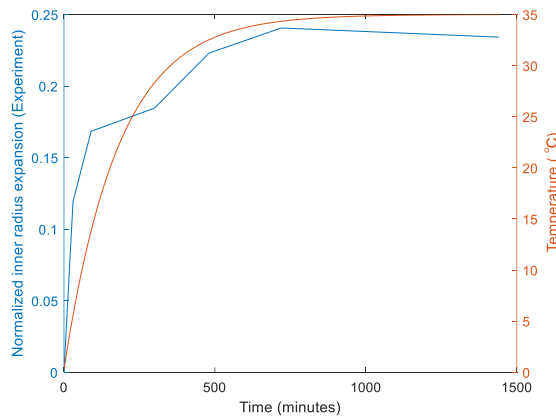


Fig.30 Comparison with temperature as function of time (calculate by b value) and experiment inner diameter expansion (The blue line is experiment inner diameter expansion; the orange line is temperature as function of time)

The heat transfer coefficient can be calculated by using the formula below ^[25],

$$hh = \frac{b\rho VC_E}{A_s} = 3.46 W/(m^2K) \quad (4.15)$$

The related values are provided in the Table 11 below.

(2) Simulation

The membrane in the experiment is PVDF and the material properties are listed in Table 11. A Part of material properties is obtained from online, the others are either given by experiment or calculate from data provided by the experiment.

Table 11 PVDF physical quantities

Property	value	
Specific Heat Capacity, C_E ^[50]	1170	J/(kg·K)
Density, ρ ^[50]	1780	kg/m ³
Elastic Modulus (25°C), E ^[46]	5×10^7	N/m ²
Poisson's Ratio, σ ^[51]	0.3	
Thermal Conductivity, k ^[46]	0.185	W/(m·K)
r_1 ⁽¹⁾	9.33×10^{-9}	m
r_N ⁽¹⁾	9.33×10^{-8}	m
Initial Temperature, T_{ini} ⁽¹⁾	273.45	K
Thermal Expansion Coefficient, α ⁽²⁾	0.0072	m/(m·K)
Heat Transfer Coefficient, hh ⁽²⁾	3.46	W/(m ² ·K)

(1) From experiment of the group (2) Hands on calculation

The α of PVDF is calculated by using the experimental data. The pore size expansion of the membrane in the experiment reached the maximum value in 12 hours and the temperature change is 34.7 °C. Therefore, α turns out to be 0.0072 m/(m·K). Because of the inner radius is nanometer scale, so the time step should be 1×10^{-4} s. The normalized inner radius expansion as function of time is shown as below.

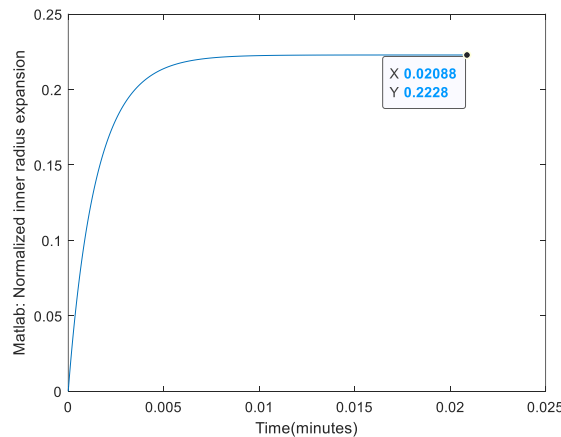


Fig.31 Normalized inner radius expansion as function of time

Comparing with the experimental result, the relative difference of normalized inner radius expansion between the simulation and the experiment is 7%. However, the time required to reach steady state has a big difference.

There are some factors to affect time required to reach steady state.

1) Adjusting the elastic modulus

As discussed before, increasing E can lead to increase of the time required to reach steady state, and E and the time required to reach steady state has a linear relationship. The time required to reach steady state with different E calculated, and the result are in the Table 12.

Table 12 Time to reach steady state under different E

E (GPa)	0.1	0.2	0.3	0.4	0.5
Time (minute)	0.03464	0.06075	0.0857	0.1099	0.1335

Therefore, by using the least squares method, the relationship between E and time to reach steady state is as follows:

$$y = 0.2x + 0.0108 \quad (4.16)$$

where y is the time required to reach steady state of the membrane in minute, x is Elastic modulus of the membrane in GPa.

Because the Elastic modulus of PVDF can be found in the range of 0.002 - 10.2 GPa ^[46], it's impossible to achieve a comparable time to reach the steady state by adjusting E of the membrane only.

2) Simulation using an equivalent hole

All the holes in membrane will be considered in the following analysis. According to the experiment, the membrane has a radius of 0.0125 m, and the porosity is 1%, so the equivalent single hole will have a radius of 0.00125 m.

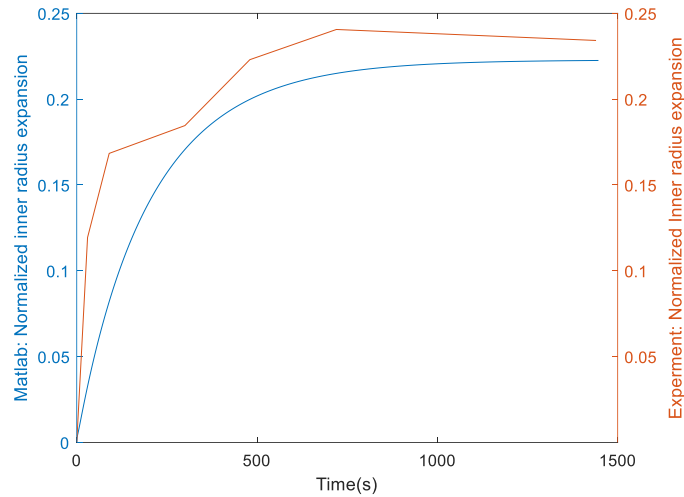


Fig.32 Comparison with nonlinear model result of normalized inner radius expansion and experiment result of normalized inner radius expansion from the group

The blue line is the simulation result of normalized inner radius expansion, and the orange line is the normalized experimental result. The inner radius expansion in two simulations has a little difference which about 7%, but the time required to reach steady state has a significant difference.

3) The effect of pore size on the time required to reach steady state

The pore size has an impact on time to reach the steady state. So, the simulation of different inner radius has been studied and the computational results are shown in Table 13.

Table 13 Time to reach steady state for different inner radii

Inner Radius (m)	$1.25 \cdot 10^{-08}$	$1.25 \cdot 10^{-07}$	$1.25 \cdot 10^{-06}$	$1.25 \cdot 10^{-05}$	$1.25 \cdot 10^{-04}$	$1.25 \cdot 10^{-03}$
Time (minute)	0.02732	0.2732	2.734	27.27	273.5	2804

It can be seen from the Table 13 that the time required to reach steady state has a linear relationship with the pore size. The larger the inner radius the longer the time required to reach steady state.

4.4 Comparing with linear elasticity model

Current study shows that α has dominate impact of inner radius expansion, but elastic properties have small influence. Moreover, E has a big influence on time to reach steady state. Thus, the nonlinear thermodynamic linear elastic model ($m=1, n=0$) will be studied and the results will be compared with those from nonlinear ($m=1, n=1$) model. Take the E as 1×10^8 Pa and time step as 10 s (because the inner radius is large so the 10 s can be used in this study), compare it with $n=0$ and $n=1$.

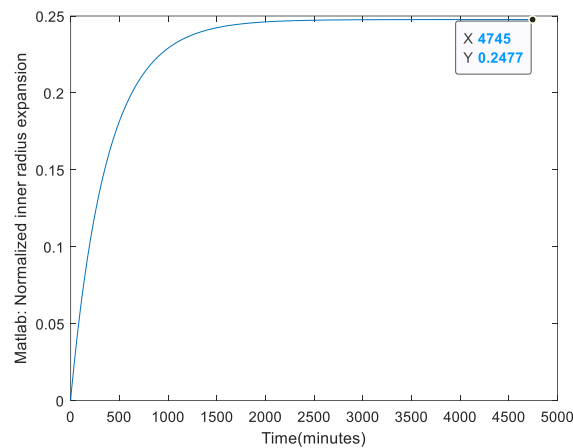


Fig.33 Normalized inner radius expansion and time to reach steady state ($n=0$)

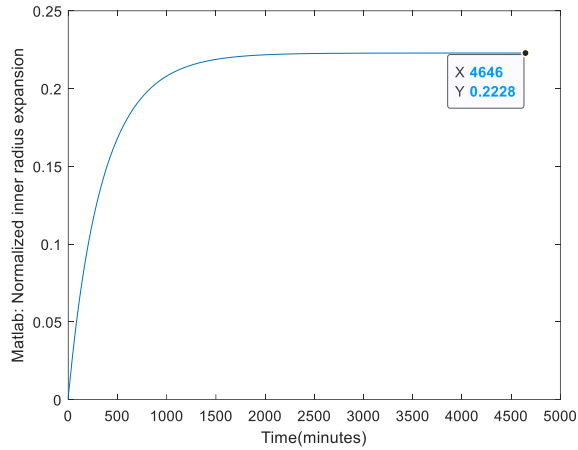


Fig.34 Normalized inner radius expansion and time to reach steady state (n=1)

From two figures, the linear elasticity model will affect the time required to reach steady state and the normalized inner radius expansion value. Linearity model will lead to a large change of the normalized inner radius expansion.

The time required to reach steady state with different E (n=0 & n=1) is shown in the Figure 35.

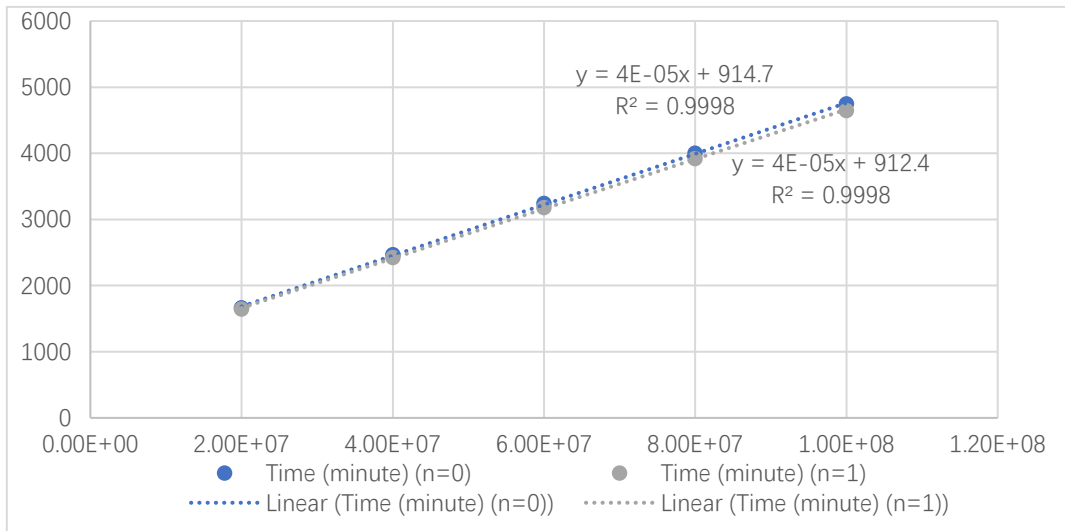


Fig.35 Comparison with n=0 and n=1 (by using increasing E value)

In both cases, the slopes of the fitted line are almost same, the intercept has small difference, but they both have a linear relationship between the time and elastic modulus.

4.5 Relationship between temperature and pore size change

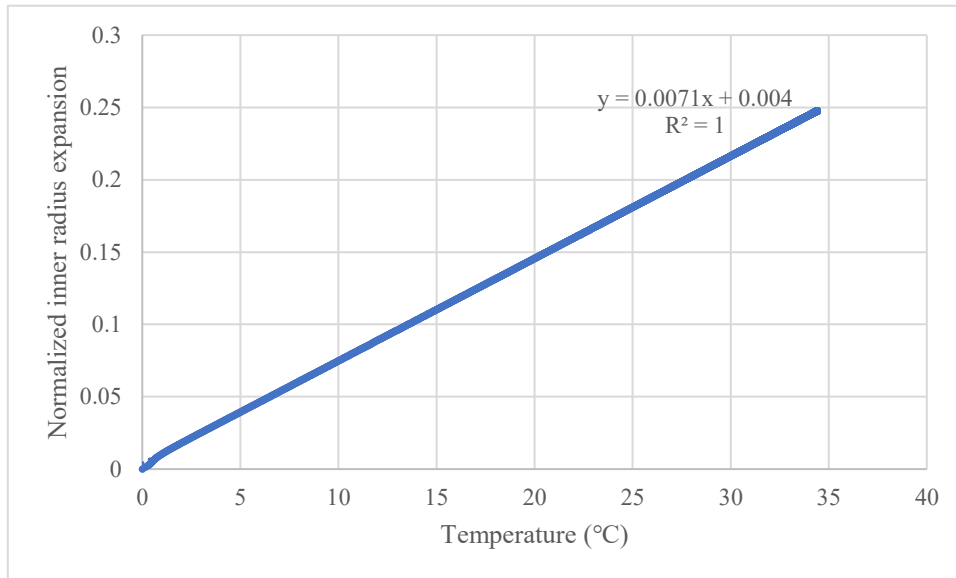


Fig.36 The normalized inner radius expansion value varies with temperature (n=0)

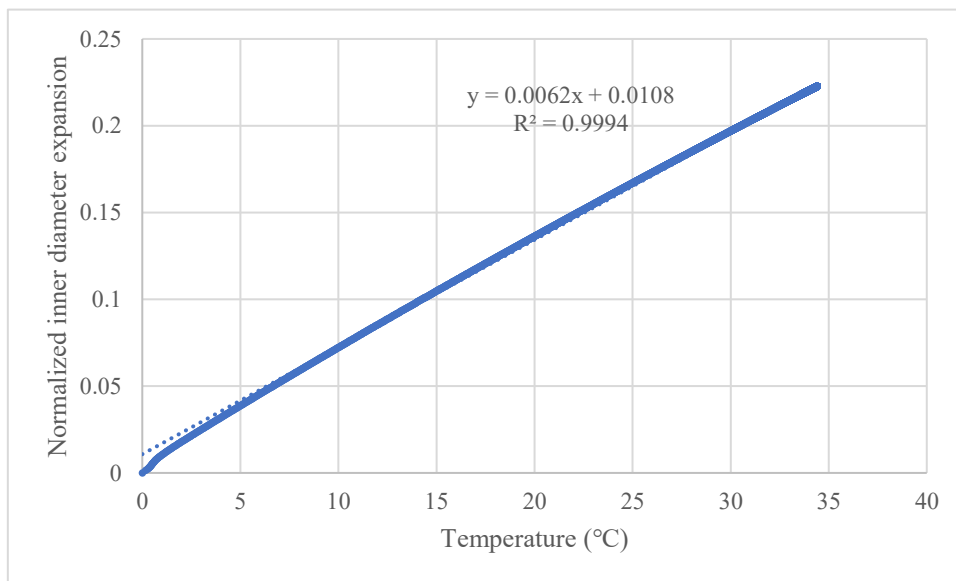


Fig.37 The normalized inner radius expansion value varies with temperature (n=1)

It is clear from Figures 36 and 37 that the inner radius expansion and temperature have a linear relationship (n=0) and almost linear relationship (n=1).

5. Conclusions

This study presents a nonlinear model that can predict the relationship between membrane pore size and temperature. This model predicts the change of membrane pore size with a change of temperature and the modeling results are in reasonably good agreement with experimental results.

Although there has a 7%-16% difference between the simulation result and two results (literature result and experiment result), it can predict the relationship between inner radius expansion and temperature. Furthermore, possible causes of errors are discussed and analyzed. Suggestions for improving the model will be discussed in the next part.

From the study, the following conclusions can be drawn:

(1) Thermal expansion coefficient (α)

The value of the α has an enormous influence on the time required to reach steady state and inner radius expansion values.

The inner diameter expansion value shows a linear relationship with the α , and as the α increases, the inner diameter expansion value also increases.

The time required to reach steady state and α show a nonlinear relationship; as the α increases, the time required to reach steady state is also increased.

(2) Heat transfer coefficient (hh)

The effect of hh on the the time required to reach steady state is nonlinear, and the larger the hh, the shorter the time to reach steady state.

(3) Elastic modulus (E)

E has a significant influence on the time required to reach steady state and it has a linear relationship with the time required to reach steady state; the larger of the E, the longer the time required to reach steady state.

(4) Pore size

The inner radius value affects the time required to reach steady state, which increases linearly as the inner radius value increases.

From the current study, the linear elasticity model (small strain, $n=0$) can predict the expansion of the inner radius. Because the thermal properties have a big influence on inner radius expansion, the model should be a nonlinear thermoelastic model ($m=1$).

6. Contributions and Improvements

6.1 Contributions

To the best of the author's knowledge, there is no mathematical model to study the pore size change of the membrane by considering both large mechanical deformation and temperature change in the literature. This model can basically predict the inner radius expansion, but the time required to reach steady state does not have a perfect adaption with the experiment. The modeling results of pore size change with temperature change are in reasonably good agreement with the experimental results.

6.2 Improvements

(1) The classical thermoelasticity has a paradox of heat conduction: the heat wave spread at an infinite speed ^[35], which is obviously contrary to the actual experimental observation. Therefore, using a hyperbolic heat transfer equation or even a non-Fourier heat conduction model is suggested in the future study.

(2) A porous thermoelasticity model may be used to improve the current model in the future study.

(3) A model considering temperature-dependent material properties should be studied in the future.

(4) Some membranes have two parts which are pedestal and membrane, so an anisotropic elastic model needs to be employed in the future study.

Reference

- [1] <https://www.worldwildlife.org/threats/water-scarcity>
- [2] VanBriesen, J. M., Dzombak, D. A., & Zhang, L. (2014) 4.19 - Sustainable Urban Water Supply Infrastructure, *Comprehensive Water Quality and Purification*. 4. 427-449, <https://doi.org/10.1016/B978-0-12-382182-9.00079-7>
- [3] Chen, T (2022). Characterization of Tertiary Membrane Fouling in Cold Climates. UWSpace. <http://hdl.handle.net/10012/17872>
- [4] <https://ourworldindata.org/grapher/un-population-projection-medium-variant>
- [5] <https://www.worldometers.info/>
- [6] <https://www.bbc.com/zhongwen/simp/science-39910567>
- [7] <https://sites.google.com/site/h20waterresources/shi-jie-que-shui-wei-ji>
- [8] <https://weatherspark.com/countries/>
- [9] Othman, N. H., Alias, N. H., Fuzil, N. S., Marpani, F., Shahrudin, M. Z., Chew, C. M., David Ng, K. M., Lau, W. J., & Ismail, A. F. (2021). A Review on the Use of Membrane Technology Systems in Developing Countries. *Membranes (Basel)*, 12(1), 30–. <https://doi.org/10.3390/membranes12010030>
- [10] Marriott, J., & Sørensen, E. (2003). A general approach to modelling membrane modules. *Chemical Engineering Science*, 58(22), 4975–4990. <https://doi.org/10.1016/j.ces.2003.07.005>
- [11] Fitzpatrick, C. S., Fradin, E., & Gregory, J. (2004). Temperature effects on flocculation, using different coagulants. *Water science and technology : a journal of the International Association on Water Pollution Research*, 50(12), 171–175. <https://pubmed.ncbi.nlm.nih.gov/15686018/>
- [12] Wilén, B.-M., Keiding, K., & Nielsen, P. H. (2000). Anaerobic deflocculation and aerobic reflocculation of activated sludge. *Water Research (Oxford)*, 34(16), 3933–3942. [https://doi.org/10.1016/S0043-1354\(00\)00274-8](https://doi.org/10.1016/S0043-1354(00)00274-8)
- [13] <https://aquarden.com/technologies/membrane-filtration/>
- [14] Lin, C.-F., Lin, T.-Y., & Hao, O. J. (2000). Effects of humic substance characteristics on UF performance. *Water Research (Oxford)*, 34(4), 1097–1106. [https://doi.org/10.1016/S0043-1354\(99\)00273-0](https://doi.org/10.1016/S0043-1354(99)00273-0)
- [15] Sillanpää, M. E. T. (2015). *Natural organic matter in water : characterization and treatment methods*. Butterworth-Heinemann, an imprint of Elsevier.
- [16] Campinas, M., Rosa, M. J. (2010). Assessing PAC contribution to the NOM fouling control in PAC/UF systems. *Water Research (Oxford)*, 44(5), 1636–1644. <https://doi.org/10.1016/j.watres.2009.11.012>
- [17] Hong, S., & Elimelech, M. (1997). Chemical and physical aspects of natural organic matter (NOM) fouling of nanofiltration membranes. *Journal of Membrane Science*, 132(2), 159–181. [https://doi.org/10.1016/S0376-7388\(97\)00060-4](https://doi.org/10.1016/S0376-7388(97)00060-4)
- [18] Lin, C.-F., Liu, S.-H., & Hao, O. J. (2001). Effect of functional groups of humic substances on uf performance. *Water Research (Oxford)*, 35(10), 2395–2402. [https://doi.org/10.1016/S0043-1354\(00\)00525-X](https://doi.org/10.1016/S0043-1354(00)00525-X)
- [19] Schäfer, A. (2001). *Natural organics removal using membranes : principles, performance and cost*. Technomic Publishing.

- [20] Bogati, R. C., Liao, B. Q., & Kam, T. (2012). Membrane fouling and its control in drinking water membrane filtration process. <https://knowledgecommons.lakeheadu.ca/handle/2453/481>
- [21] Ogbonna. C. B., Berebon. D. P., & Onwuegbu. E. K. (2015). Relationship between Temperature, Ph and Population of Selected Microbial Indicators during Anaerobic Digestion of Guinea Grass (*Panicum Maximum*), *American Journal of Microbiological Research*, vol. 3, no.1, pp. 14-24, <http://pubs.sciepub.com/ajmr/3/1/3>
- [22] Shu, L., Obagbemi, I. J., Liyanaarachchi, S., Navaratna, D., Parthasarathy, R., Aim, R. B., & Jegatheesan, V. (2016). Why does pH increase with CaCl₂ as draw solution during forward osmosis filtration. *Process Safety and Environmental Protection*, 104, 465–471. <https://doi.org/10.1016/j.psep.2016.06.007>
- [23] Lepane, V., Depret, L., Väli, A.-L., & Suursööt, K. (2015). Impact of seasonal climate change on optical and molecular properties of river water dissolved organic matter by HPLC-SEC and UV-vis spectroscopy. *Chemical and Biological Technologies in Agriculture*, 2(1), 1–. <https://doi.org/10.1186/s40538-015-0040-6>
- [24] Ma, C., Yu, S. L., Shi, W. X., Heijman, S. G. J., & Rietveld, L.C. (2013). Effect of different temperatures on performance and membrane fouling in high concentration PAC–MBR system treating micro-polluted surface water. *Bioresource Technology*, 141, 19–24. <https://doi.org/10.1016/j.biortech.2013.02.025>
- [26] Guerrero, R., Rubio Rosas, E., & Rodriguez Lugo. (2010). Nonlinear changes in pore size induced by temperature in the design of smart membranes. *Polymer Journal*, 42, 947–951. <https://doi.org/10.1038/pj.2010.88>
- [25] Hughes, A.J., Mallick, T. K., & O'Donovan, T. S. (2020). Investigation of the Effects of Temperature on the Microstructure of PTFE Microfiltration Membranes Under Membrane Distillation Conditions. *Journal of Advanced Thermal Science Research*, 7(1), 11–21. <https://doi.org/10.15377/2409-5826.2020.07.2>
- [27] Rizki, Z., Suryawirawan, E., Janssen, A. E. M., van der Padt, A., & Boom, R. M. (2020). Modelling temperature effects in a membrane cascade system for oligosaccharides. *Journal of Membrane Science*, 610, 118292. <https://doi.org/10.1016/j.memsci.2020.118292>
- [28] Fan, G, D., Lin, R, J., & Wei, Z, Q. (2016). Research on the efficiency of ultrafiltration integrated device for treating Minjiang water in low temperature period. *China Water Supply and Drainage*, pp:51-55. <https://doi.org/10.19853/j.zgjsps.1000-4602.2016.17.011>
- [29] Shen, B., Wu, Y., & Wang, L. (2013). The research and application of ultra-filtration water purification process at low temperature in cold area. *Drinking water safety control technology conference and the 13th annual meeting of the Water Supply Committee of the Water Industry Branch of the Chinese Civil Engineering Society*, 17, 286-295. <https://kns.cnki.net/kcms/detail/detail.aspx?FileName=OGTY201309002034&DbName=CPFD2014>
- [30] https://www.bh1978.com/shuiguolv_153922
- [31] Mohammad, A. Wahab. (2002). A Modified Donnan-Steric-Pore Model for Predicting Flux and Rejection of dye/NaCl Mixture in Nanofiltration Membranes.

Separation Science and Technology, 37(5), 1009–29. <https://doi.org/10.1081/SS-120002238>.

[32] Bowen, W.R., & Welfoot, J. S. (2002). Modelling the performance of membrane nanofiltration—critical assessment and model development. *Chemical Engineering Science*, 57(7), 1121–1137. [https://doi.org/10.1016/S0009-2509\(01\)00413-4](https://doi.org/10.1016/S0009-2509(01)00413-4)

[33] Mukhopadhyay, S., Picard, R., Trostorff, S., Waurick, M. (2016). On some models in linear thermo-elasticity with rational material laws. *Mathematics and Mechanics of Solids*, 21(9), 1149–1163. <https://doi.org/10.1177/1081286514556014>

[34] Mukhopadhyay, Picard, R., Trostorff, S., & Waurick, M. (2017). A note on a two-temperature model in linear thermoelasticity. *Mathematics and Mechanics of Solids*, 22(5), 905–918. <https://doi.org/10.1177/1081286515611947>

[35] Zhang, H. L., Kim, S., Choi, G., Xie, D. M., & Cho, H. H. (2021). Analysis of thermoelastic problems in isotropic solids undergoing large temperature changes based on novel models of thermoelasticity. *International Journal of Heat and Mass Transfer*, 177, 121576–. <https://doi.org/10.1016/j.ijheatmasstransfer.2021.121576>

[36] Ehsan, T., Molaei Najafabadi, M., & Reddy, J. (2014). Size-dependent generalized thermoelasticity model for Timoshenko micro-beams based on strain gradient and non-Fourier heat conduction theories. *Composite Structures*, 116, 595–611. <https://doi.org/10.1016/j.compstruct.2014.05.040>

[37] Siddhartha, B. (2019). Fundamental solution of steady oscillations for porous materials with dual-phase-lag model in micropolar thermoelasticity. *Mechanics Based Design of Structures and Machines*, 47(4), 430–452. <https://doi.org/10.1080/15397734.2018.1557528>

[38] Chatterjee, A. N., Yu, Q., Moore, J. S., & Aluru, N. R. (2003). Mathematical Modeling and Simulation of Dissolvable Hydrogels. *Journal of Aerospace Engineering*, 16(2), 55–64. [https://doi.org/10.1061/\(ASCE\)0893-1321\(2003\)16:2\(55\)](https://doi.org/10.1061/(ASCE)0893-1321(2003)16:2(55))

[39] Park, Y., Gutierrez, M. P., & Lee, L. P. (2016). Reversible Self-Actuated Thermo-Responsive Pore Membrane. *Scientific Reports*, 6(1), 39402–39402. <https://doi.org/10.1038/srep39402>

[40] Katsikadelis, J.T. 2002. Boundary elements: theory and applications. Elsevier, New York.

[41]

https://en.wikipedia.org/wiki/Boundary_element_method#CITEREFKatsikadelis2002

[42]

https://en.wikipedia.org/wiki/Finite_element_method#Comparison_to_the_finite_difference_method

[43] <https://zhuanlan.zhihu.com/p/109231996>

[44] https://en.wikipedia.org/wiki/Finite_difference_method

[45] Crank, J., & Nicolson, P. (1947). "A practical method for numerical evaluation of solutions of partial differential equations of the heat conduction type". *Proc. Camb. Phil. Soc.* 43 (1): 50–67. <https://doi.org/10.1017/S0305004100023197>

[46] <https://www.matweb.com/>

[47] Vavlekas, D., Melo, L., Ansari, M., Grant, E., Fremy, F., McCoy, J. L., & Hatzikiriakos, S. G. (2017). Role of PTFE paste fibrillation on Poisson's ratio. *Polymer Testing*, 61, 65–73. <https://doi.org/10.1016/j.polymertesting.2017.05.004>

- [48] Price, D. M., & Jarratt, M. (2002). Thermal conductivity of PTFE and PTFE composites. *Thermochimica Acta*, 392-393(C), 231–236. [https://doi.org/10.1016/S0040-6031\(02\)00105-3](https://doi.org/10.1016/S0040-6031(02)00105-3)
- [49] dos Santos, W. N., Iguchi, C., & Gregorio, R. (2008). Thermal properties of poly (vinilidene fluoride) in the temperature range from 25 to 210°C. *Polymer Testing*, 27(2), 204–208. <https://doi.org/10.1016/j.polymertesting.2007.10.005>
- [50] <http://www.sellpa6.com/news-1-3533.html>
- [51] <http://www.chinagtec.com/2/2021-01-07/28678.html>

Appendix 1 Average Temperatures in High Latitudes Countries

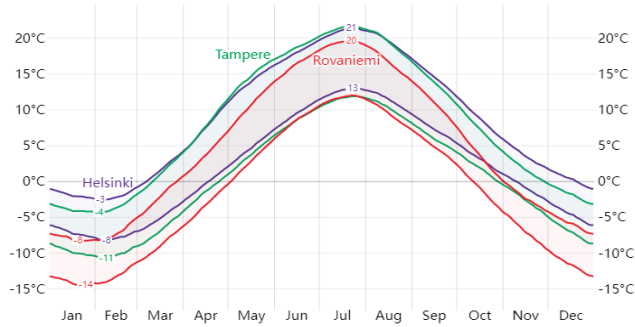


Fig.3-b Average High and Low Temperature in Finland

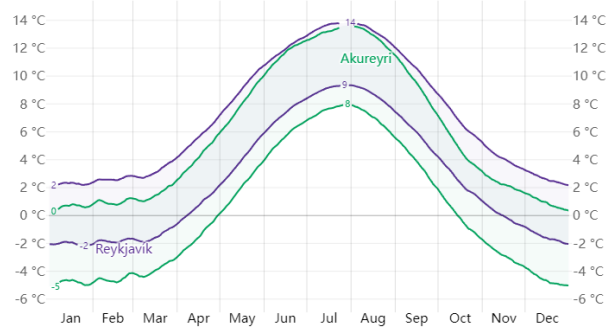


Fig.3-c Average High and Low Temperature in Iceland

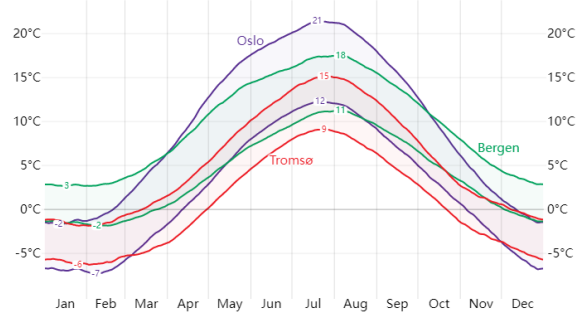


Fig.3-d Average High and Low Temperature in Norway

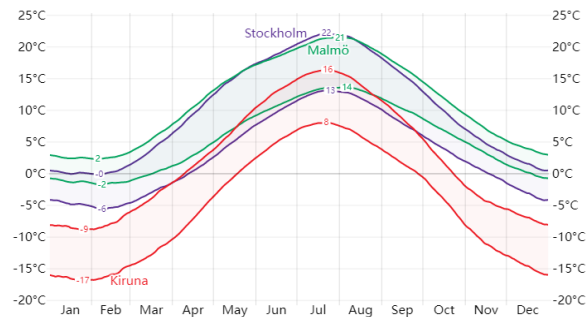


Fig.3-e Average High and Low Temperature in Sweden

Appendix 2 Pseudo Code and Stopping Criteria

Pseudo Code:

Prepare data

Prepare FD information (h and $\Delta t, k_{\max}, \varepsilon_{ur}, \varepsilon_{ua}, \varepsilon_{rr}, \varepsilon_{ra}$)

Let $w(j)$ be the solution at time $t_j = (j-1)\Delta t$ for $j = 1, 2, \dots, M$.

Then $w(1)$ is the initial conditions.

For j from 1 to $M-1$ (loop over time)

Initial guess $w^- = w(j)$, Of course, $w(1)$ is the initial condition.

Calculate the norm of w^- and $G(w^-)$

For k from 1 to k_{\max} ... Newton method to find $w(j+1)$

Calculate the Jacobian of the system G at the initial guess:

$$J_{pq}(w^-) = \frac{\partial G_p}{\partial w_q}(w^-)$$

Solve $J(w^-)\delta w = -G(w^-)$

Find the approximate solution $w = w^- + \delta w$

Update the initial guess by w .

Calculate the norm of δw and $G(w)$ to check if convergency is reached

(see stopping criteria).

End of Newton Iteration

Update $w(j+1) = w$

Save $w(j+1)$ to a matrix W , each column of W :

$$W = [w(1), w(2), \dots, w(j), \dots, w(M)].$$

End of solution

Stopping Criteria

$$\|G(w)\| \leq \varepsilon_{rr} \|G(w_0)\| + \varepsilon_{ra}$$

where $\|\cdot\|$ is the standard Euclidean vector norm, w_0 is the start value of w^- , ε_{rr} is the tolerance in the relative criterion and ε_{ra} is the tolerance in the absolute criterion.

To prevent divergent iterations to run forever, one terminates the iterations when the current number of iterations k exceeds a maximum value k_{max} .

With the change in solution as criterion we can formulate a combined absolute and relative measure of the change in the solution:

$$\|\delta w\| \leq \varepsilon_{ur} \|w_0\| + \varepsilon_{ua}$$

The ultimate termination criterion, combining the residual and the change in solution with a test on the maximum number of iterations, can be expressed as:

$$\|G(w)\| \leq \varepsilon_{rr} \|G(w_0)\| + \varepsilon_{ra} \text{ or } \|\delta w\| \leq \varepsilon_{ur} \|w_0\| + \varepsilon_{ua} \text{ or } k > k_{max}.$$

Appendix 3 Jacobian Matrix

function Jacob=Jacob()

global dt Tref nv N H S1 S2 S3 S4 S5 kh n m r u v T u00 v00 uN01 vN01 lamda Bj0

```

% u0
Du0Du1=((4 * H ^ 2 * nv + 9 * r(1) ^ 2) * u(1) / r(1) ^ 2 / H) / 0.2e1 - (6 * u(2) /
H) + 0.3e1 / 0.2e1 * u(3) / H) * n + (2 * H * nv / r(1));
Du0Du2=(-6 / H * u(1) + 8 * u(2) / H - 2 * u(3) / H) * n + 1;
Du0Du3=(0.3e1 / 0.2e1 / H * u(1) - 0.2e1 * u(2) / H + u(3) / H / 0.2e1) * n;
Du0DT1=-2 * S5 * H;
Du0DT2=0;
Du0Dv1=0;
Du0Dv2=0;
Du0Dv3=0;

% v0
Dv0Du1=((4 * H ^ 2 * nv + 9 * r(1) ^ 2) * v(1) / r(1) ^ 2 / H) / 0.2e1 - (6 * v(2) /
H) + 0.3e1 / 0.2e1 * v(3) / H) * n;
Dv0Du2=(-6 * v(1) / H + 8 * v(2) / H - 2 * v(3) / H) * n;
Dv0Du3=(0.3e1 / 0.2e1 * v(1) / H - 0.2e1 * v(2) / H + v(3) / H / 0.2e1) * n;
Dv0Dv1=((4 * H ^ 2 * nv + 9 * r(1) ^ 2) * u(1) / r(1) ^ 2 / H) / 0.2e1 - (6 * u(2) /
H) + 0.3e1 / 0.2e1 * u(3) / H) * n + (2 * H * nv / r(1));
Dv0Dv2=(-6 / H * u(1) + 8 * u(2) / H - 2 * u(3) / H) * n + 1;
Dv0Dv3=(0.3e1 / 0.2e1 / H * u(1) - 0.2e1 * u(2) / H + u(3) / H / 0.2e1) * n;

% T0
DT0DT1=2 * H / kh;
DT0DT2=1;

% un1
Dun1Dunm2=(-u(N - 2) / H / 0.2e1 + 0.2e1 * u(N - 1) / H - 0.3e1 / 0.2e1 * u(N) /
H) * n;
Dun1Dunm1=(2 * u(N - 2) / H - 8 * u(N - 1) / H + 6 * u(N) / H) * n + 1;
Dun1Dun=(-0.3e1 / 0.2e1 * u(N - 2) / H + 0.6e1 * u(N - 1) / H + (-0.4e1 * H ^ 2
* nv - (9 * r(N) ^ 2)) * u(N) / H / (r(N) ^ 2) / 0.2e1) * n - 0.2e1 * H * nv / r(N);
Dun1DTn= 2 * S5 * H;
Dun1Dvnm2=0;
Dun1Dvnm1=0;
Dun1Dvn=0;

% vn1

```

```

Dvn1Dunm2=((2 * v(N - 1) / H) - 0.3e1 / 0.2e1 * v(N) / H - (v(N - 2) / H) / 0.2e1)
* n;
Dvn1Dunm1=(-8 * v(N - 1) / H + 6 * v(N) / H + 2 * v(N - 2) / H) * n;
Dvn1Dun=((6 * v(N - 1) / H) + ((-4 * H ^ 2 * nv - 9 * r(N) ^ 2) * v(N) / H / r(N)
^ 2) / 0.2e1 - 0.3e1 / 0.2e1 * v(N - 2) / H) * n;
Dvn1Dvnm2=(-u(N - 2) / H / 0.2e1 + 0.2e1 * u(N - 1) / H - 0.3e1 / 0.2e1 * u(N) /
H) * n;
Dvn1Dvnm1=(2 * u(N - 2) / H - 8 * u(N - 1) / H + 6 * u(N) / H) * n + 1;
Dvn1Dvn=(-0.3e1 / 0.2e1 * u(N - 2) / H + 0.6e1 * u(N - 1) / H + (-0.4e1 * H ^ 2
* nv - (9 * r(N) ^ 2)) * u(N) / H / (r(N) ^ 2) / 0.2e1) * n - 0.2e1 * H * nv / r(N);

% Tn1
DTn1DTnm1=1;
DTn1DTn=2 * H / kh;
DTn1Dun1=0;
DTn1Dvn1=0;

% F21
DF21Du0=(-u(1) * nv / r(1) ^ 2 / H / 0.2e1 + (0.1e1 - nv) * (u00 - u(2)) / r(1) / H
^ 2 / 0.4e1 + (-0.2e1 * u00 + 0.2e1 * u(1)) / H ^ 3 / 0.2e1) * S1 * n + (0.1e1 / H ^ 2 -
0.1e1 / H / r(1) / 0.2e1) * S1;
DF21DT0=S2 / H / 0.2e1;
DF21Du1=-((1 + nv) * u(1) / r(1) ^ 3) + ((u(2) - u00) * nv / r(1) ^ 2 / H) / 0.2e1
+ ((2 * u00 - 2 * u(2)) / H ^ 3) / 0.2e1) * S1 * n + (-2 / H ^ 2 - 1 / r(1) ^ 2) * S1;
DF21Du2=(u(1) * nv / r(1) ^ 2 / H / 0.2e1 - (0.1e1 - nv) * (u00 - u(2)) / r(1) / H ^
2 / 0.4e1 + (-0.2e1 * u(1) + 0.2e1 * u(2)) / H ^ 3 / 0.2e1) * S1 * n + (0.1e1 / H ^ 2 +
0.1e1 / H / r(1) / 0.2e1) * S1;
DF21DT2=-S2 / H / 0.2e1;

% F2N
DF2nDun1=(u(N) * nv / H / r(N) ^ 2 / 0.2e1 - (0.1e1 - nv) * (u(N - 1) - uN01) /
r(N) / H ^ 2 / 0.4e1 + (-0.2e1 * u(N) + 0.2e1 * uN01) / H ^ 3 / 0.2e1) * S1 * n + (0.1e1
/ H ^ 2 + 0.1e1 / H / r(N) / 0.2e1) * S1;
DF2nDTn1=-S2 / H / 0.2e1;
DF2nDunm1=(-u(N) * nv / H / r(N) ^ 2 / 0.2e1 + (0.1e1 - nv) * (u(N - 1) - uN01)
/ r(N) / H ^ 2 / 0.4e1 + (0.2e1 * u(N) - 0.2e1 * u(N - 1)) / H ^ 3 / 0.2e1) * S1 * n +
(0.1e1 / H ^ 2 - 0.1e1 / H / r(N) / 0.2e1) * S1;
DF2nDun=-((1 + nv) * u(N) / r(N) ^ 3) + ((uN01 - u(N - 1)) * nv / H / r(N) ^ 2) /
0.2e1 + ((2 * u(N - 1) - 2 * uN01) / H ^ 3) / 0.2e1) * S1 * n + (-2 / H ^ 2 - 1 / r(N) ^ 2)
* S1;
DF2nDTnm1=S2 / H / 0.2e1;

% F31

```

$$DF31Du0 = -((v00 - v(2)) * T(1) * S3 * m / H^2 / Tref / 0.4e1 + (v00 - v(2)) * S3 / H^2 / 0.4e1) * n;$$

$$DF31Dv0 = -((u00 / H^2 / 0.4e1 - u(2) / H^2 / 0.4e1) * T(1) * S3 * m / Tref + (u00 / H^2 / 0.4e1 - u(2) / H^2 / 0.4e1) * S3) * n + T(1) * S3 * m / H / Tref / 0.2e1 + S3 / H / 0.2e1;$$

$$DF31DT0 = -(-0.1e1 / H^2 + 0.1e1 / H / r(1) / 0.2e1) * S4;$$

$$DF31Du1 = -(v(1) * T(1) * S3 * m / r(1)^2 / Tref + v(1) * S3 / r(1)^2) * n;$$

$$DF31Dv1 = -(u(1) * T(1) * S3 * m / r(1)^2 / Tref + u(1) * S3 / r(1)^2) * n - T(1) * S3 * m / r(1) / Tref - S3 / r(1);$$

$$DF31DT1 = -((v00 - v(2)) * u00 / H^2 / 0.4e1 + v(1) * u(1) / r(1)^2 + (-v00 + v(2)) * u(2) / H^2 / 0.4e1) * S3 * m * n / Tref - (-v00 / H / 0.2e1 + v(2) / H / 0.2e1 + v(1) / r(1)) * S3 * m / Tref - 0.2e1 * S4 / H^2;$$

$$DF31Du2 = -((-v00 + v(2)) * T(1) * S3 * m / H^2 / Tref / 0.4e1 + (-v00 + v(2)) * S3 / H^2 / 0.4e1) * n;$$

$$DF31Dv2 = -((-u00 / H^2 / 0.4e1 + u(2) / H^2 / 0.4e1) * T(1) * S3 * m / Tref + (-u00 / H^2 / 0.4e1 + u(2) / H^2 / 0.4e1) * S3) * n - T(1) * S3 * m / H / Tref / 0.2e1 - S3 / H / 0.2e1;$$

$$DF31DT2 = -(-0.1e1 / H^2 - 0.1e1 / H / r(1) / 0.2e1) * S4;$$

$$DF31Du3 = 0;$$

$$DF31Dv3 = 0;$$

$$DF31DT3 = 0;$$

% F3N

$$DF3nDunm1 = -((v(N - 1) - vN01) * T(N) * S3 * m / H^2 / Tref / 0.4e1 + (v(N - 1) - vN01) * S3 / H^2 / 0.4e1) * n;$$

$$DF3nDvnm1 = -((u(N - 1) / H^2 / 0.4e1 - uN01 / H^2 / 0.4e1) * T(N) * S3 * m / Tref + (u(N - 1) / H^2 / 0.4e1 - uN01 / H^2 / 0.4e1) * S3) * n + T(N) * S3 * m / H / Tref / 0.2e1 + S3 / H / 0.2e1;$$

$$DF3nDTnm1 = -(-0.1e1 / H^2 + 0.1e1 / H / r(N) / 0.2e1) * S4;$$

$$DF3nDun = -(v(N) * T(N) * S3 * m / r(N)^2 / Tref + v(N) * S3 / r(N)^2) * n;$$

$$DF3nDvn = -(u(N) * T(N) * S3 * m / r(N)^2 / Tref + u(N) * S3 / r(N)^2) * n - T(N) * S3 * m / r(N) / Tref - S3 / r(N);$$

$$DF3nDTn = -((v(N - 1) - vN01) * u(N - 1) / H^2 / 0.4e1 + v(N) * u(N) / r(N)^2 + (-v(N - 1) + vN01) * uN01 / H^2 / 0.4e1) * S3 * m * n / Tref - (-v(N - 1) / H / 0.2e1 + vN01 / H / 0.2e1 + v(N) / r(N)) * S3 * m / Tref - 0.2e1 * S4 / H^2;$$

$$DF3nDun1 = -((-v(N - 1) + vN01) * T(N) * S3 * m / H^2 / Tref / 0.4e1 + (-v(N - 1) + vN01) * S3 / H^2 / 0.4e1) * n;$$

$$DF3nDvn1 = -((-u(N - 1) / H^2 / 0.4e1 + uN01 / H^2 / 0.4e1) * T(N) * S3 * m / Tref + (-u(N - 1) / H^2 / 0.4e1 + uN01 / H^2 / 0.4e1) * S3) * n - T(N) * S3 * m / H / Tref / 0.2e1 - S3 / H / 0.2e1;$$

$$DF3nDTn1 = -(-0.1e1 / H^2 - 0.1e1 / H / r(N) / 0.2e1) * S4;$$

for i=2:N-1

```

% F2i
DF2iDui1=(u(i) * nv / r(i) ^ 2 / H / 0.2e1 - (0.1e1 - nv) * (u(i - 1) - u(i + 1)) /
r(i) / H ^ 2 / 0.4e1 + (-0.2e1 * u(i) + 0.2e1 * u(i + 1)) / H ^ 3 / 0.2e1) * S1 * n + (0.1e1
/ H ^ 2 + 0.1e1 / H / r(i) / 0.2e1) * S1;
DF2iDTi1=-S2 / H / 0.2e1;
DF2iDuim1=(-u(i) * nv / r(i) ^ 2 / H / 0.2e1 + (0.1e1 - nv) * (u(i - 1) - u(i + 1))
/ r(i) / H ^ 2 / 0.4e1 + (0.2e1 * u(i) - 0.2e1 * u(i - 1)) / H ^ 3 / 0.2e1) * S1 * n + (0.1e1
/ H ^ 2 - 0.1e1 / H / r(i) / 0.2e1) * S1;
DF2iDui=-((1 + nv) * u(i) / r(i) ^ 3) + ((u(i + 1) - u(i - 1)) * nv / r(i) ^ 2 / H) /
0.2e1 + ((2 * u(i - 1) - 2 * u(i + 1)) / H ^ 3) / 0.2e1) * S1 * n + (-2 / H ^ 2 - 1 / r(i) ^ 2)
* S1;
DF2iDTim1= S2 / H / 0.2e1;
DF2iDTi=0;

```

```

% F3i
DF3iDuim1=-((v(i - 1) - v(i + 1)) * T(i) * S3 * m / H ^ 2 / Tref / 0.4e1 + (v(i -
1) - v(i + 1)) * S3 / H ^ 2 / 0.4e1) * n;
DF3iDvim1= -((u(i - 1) / H ^ 2 / 0.4e1 - u(i + 1) / H ^ 2 / 0.4e1) * T(i) * S3 * m
/ Tref + (u(i - 1) / H ^ 2 / 0.4e1 - u(i + 1) / H ^ 2 / 0.4e1) * S3) * n + T(i) * S3 * m / H
/ Tref / 0.2e1 + S3 / H / 0.2e1;
DF3iDTim1=-(-0.1e1 / H ^ 2 + 0.1e1 / H / r(i) / 0.2e1) * S4;
DF3iDui=-v(i) * T(i) * S3 * m / r(i) ^ 2 / Tref + v(i) * S3 / r(i) ^ 2) * n;
DF3iDvi=-u(i) * T(i) * S3 * m / r(i) ^ 2 / Tref + u(i) * S3 / r(i) ^ 2) * n - T(i) *
S3 * m / r(i) / Tref - S3 / r(i);
DF3iDTi=-((v(i - 1) - v(i + 1)) * u(i - 1) / H ^ 2 / 0.4e1 + v(i) * u(i) / r(i) ^ 2 +
(-v(i - 1) + v(i + 1)) * u(i + 1) / H ^ 2 / 0.4e1) * S3 * m * n / Tref - (-v(i - 1) / H / 0.2e1
+ v(i + 1) / H / 0.2e1 + v(i) / r(i)) * S3 * m / Tref - 0.2e1 * S4 / H ^ 2;
DF3iDui1=-((-v(i - 1) + v(i + 1)) * T(i) * S3 * m / H ^ 2 / Tref / 0.4e1 + (-v(i -
1) + v(i + 1)) * S3 / H ^ 2 / 0.4e1) * n;
DF3iDvi1=-((-u(i - 1) / H ^ 2 / 0.4e1 + u(i + 1) / H ^ 2 / 0.4e1) * T(i) * S3 * m
/ Tref + (-u(i - 1) / H ^ 2 / 0.4e1 + u(i + 1) / H ^ 2 / 0.4e1) * S3) * n - T(i) * S3 * m / H
/ Tref / 0.2e1 - S3 / H / 0.2e1;
DF3iDTi1=-(-0.1e1 / H ^ 2 - 0.1e1 / H / r(i) / 0.2e1) * S4;

```

```

% ??

```

```

J(3*i-2,3*i-2)=1;
J(3*i-2,3*i-1)=-lamda*dt;
J(3*i-2,3*i)=0;

```

```

J(3*i-1,3*i-5)=-lamda*dt*DF2iDuim1;
J(3*i-1,3*i-4)=0;
J(3*i-1,3*i-3)=-lamda*dt*DF2iDTim1;
J(3*i-1,3*i-2)=-lamda*dt*DF2iDui;
J(3*i-1,3*i-1)=1;

```

```

J(3*i-1,3*i )=-lamda*dt*DF2iDTi;
J(3*i-1,3*i+1)=-lamda*dt*DF2iDui1;
J(3*i-1,3*i+2)=0;
J(3*i-1,3*i+3)=-lamda*dt*DF2iDTi1;

J(3*i,3*i-5)=-lamda*dt*DF3iDuim1;
J(3*i,3*i-4)=-lamda*dt*DF3iDvim1;
J(3*i,3*i-3)=-lamda*dt*DF3iDTim1;
J(3*i,3*i-2)=-lamda*dt*DF3iDui;
J(3*i,3*i-1)=-lamda*dt*DF3iDvi;
J(3*i,3*i )=Bj0(i)-lamda*dt*DF3iDTi;
J(3*i,3*i+1)=-lamda*dt*DF3iDui1;
J(3*i,3*i+2)=-lamda*dt*DF3iDvi1;
J(3*i,3*i+3)=-lamda*dt*DF3iDTi1;
end

% ???
J(1,1)=1;
J(1,2)=-lamda*dt;
J(1,3)=0;

J(2,1)=-lamda*dt*(DF21Du0*Du0Du1+DF21Du1);
J(2,2)=1;
J(2,3)=-lamda*dt*(DF21Du0*Du0DT1+DF21DT0*DT0DT1);
J(2,4)=-lamda*dt*(DF21Du0*Du0Du2+DF21Du2);
J(2,5)=0;
J(2,6)=-lamda*dt*(DF21Du0*Du0DT2+DF21DT0*DT0DT2+DF21DT2);
J(2,7)=-lamda*dt*(DF21Du0*Du0Du3);
J(2,8)=0;
J(2,9)=0;

J(3,1)=-lamda*dt*(DF31Du0*Du0Du1+DF31Dv0*Dv0Du1+DF31Du1);
J(3,2)=-lamda*dt*(DF31Du0*Du0Dv1+DF31Dv0*Dv0Dv1+DF31Dv1);
J(3,3)=Bj0(1)-lamda*dt*(DF31Du0*Du0DT1+DF31DT0*DT0DT1+DF31DT1);
J(3,4)=-lamda*dt*(DF31Du0*Du0Du2+DF31Dv0*Dv0Du2+DF31Du2);
J(3,5)=-lamda*dt*(DF31Du0*Du0Dv2+DF31Dv0*Dv0Dv2+DF31Dv2);
J(3,6)=-lamda*dt*(DF31DT0*DT0DT2+DF31DT2);
J(3,7)=-lamda*dt*(DF31Du0*Du0Du3+DF31Dv0*Dv0Du3+DF31Du3);
J(3,8)=-lamda*dt*(DF31Du0*Du0Dv3+DF31Dv0*Dv0Dv3+DF31Dv3);
J(3,9)=-lamda*dt*(DF31DT3);

% i=N
J(3*N-2,3*N-2)=1;

```

```

J(3*N-2,3*N-1)=-lamda*dt;
J(3*N-2,3*N )=0;

J(3*N-1,3*N-8)=-lamda*dt*(DF2nDun1*Dun1Dunm2);
J(3*N-1,3*N-7)=0;
J(3*N-1,3*N-6)=0;
J(3*N-1,3*N-5)=-lamda*dt*(DF2nDun1*Dun1Dunm1+DF2nDunm1);
J(3*N-1,3*N-4)=0;
J(3*N-1,3*N-3)=-lamda*dt*(DF2nDTn1*DTn1DTnm1+DF2nDTnm1);
J(3*N-1,3*N-2)=-lamda*dt*(DF2nDun1*Dun1Dun+DF2nDun);
J(3*N-1,3*N-1)=1;
J(3*N-1,3*N )=-lamda*dt*(DF2nDTn1*DTn1DTn);

J(3*N,3*N-8)=-lamda*dt*(DF3nDun1*Dun1Dunm2+DF3nDvn1*Dvn1Dunm2);
J(3*N,3*N-7)=-lamda*dt*(DF3nDun1*Dun1Dvnm2+DF3nDvn1*Dvn1Dvnm2);
J(3*N,3*N-6)=0;
J(3*N,3*N-5)=-
lamda*dt*(DF3nDun1*Dun1Dunm1+DF3nDvn1*Dvn1Dunm1+DF3nDunm1);
J(3*N,3*N-4)=-
lamda*dt*(DF3nDun1*Dun1Dvnm1+DF3nDvn1*Dvn1Dvnm1+DF3nDvnm1);
J(3*N,3*N-3)=-lamda*dt*(DF3nDTn1*DTn1DTnm1+DF3nDTnm1);
J(3*N,3*N-2)=-
lamda*dt*(DF3nDun1*Dun1Dun+DF3nDvn1*Dvn1Dun+DF3nDun);
J(3*N,3*N-1)=-
lamda*dt*(DF3nDun1*Dun1Dvn+DF3nDvn1*Dvn1Dvn+DF3nDvn);
J(3*N,3*N )=-lamda*dt*(DF3nDTn1*DTn1DTn+DF3nDTn);
)=-Bj0(N)-

Jacob=J;
end

```

Appendix 4 F2i and F3i

$$F21 = -((1 + nv) * u1^2 / r1^3) / 0.2e1 + (u1 * (u2 - u0) * nv / r1^2 / H) / 0.2e1 + ((1 - nv) * (u0 - u2)^2 / r1 / H^2) / 0.8e1 + ((-u0^2 + 2 * u0 * u1 - 2 * u1 * u2 + u2^2) / H^3) / 0.2e1 * S1 * n + (((u2 - 2 * u1 + u0) / H^2) + ((u2 - u0) / H / r1)) / 0.2e1 - (u1 / r1^2) * S1 + (S2 * (T0 - T2) / H) / 0.2e1;$$

$$F2i = -((1 + nv) * ui^2 / ri^3) / 0.2e1 + (ui * (ui1 - uim1) * nv / ri^2 / H) / 0.2e1 + ((1 - nv) * (uim1 - ui1)^2 / ri / H^2) / 0.8e1 + ((2 * ui * uim1 - 2 * ui * ui1 - uim1^2 + ui1^2) / H^3) / 0.2e1 * S1 * n + (((ui1 - 2 * ui + uim1) / H^2) + ((ui1 - uim1) / H / ri)) / 0.2e1 - (ui / ri^2) * S1 + ((TIM1 - TI1) * S2 / H) / 0.2e1;$$

$$F2N = -((1 + nv) * un^2 / rn^3) / 0.2e1 + (un * (un1 - unm1) * nv / H / rn^2) / 0.2e1 + ((1 - nv) * (unm1 - un1)^2 / rn / H^2) / 0.8e1 + ((2 * un * unm1 - 2 * un * un1 - unm1^2 + un1^2) / H^3) / 0.2e1 * S1 * n + (((un1 - 2 * un + unm1) / H^2) + ((un1 - unm1) / H / rn)) / 0.2e1 - (un / rn^2) * S1 + ((TNM1 - TN1) * S2 / H) / 0.2e1;$$

$$F31 = -((v0 - v2) * u0 / H^2 / 0.4e1 + v1 * u1 / r1^2 + (-v0 + v2) * u2 / H^2 / 0.4e1) * T1 * S3 * m / Tref + ((v0 - v2) * u0 / H^2 / 0.4e1 + v1 * u1 / r1^2 + (-v0 + v2) * u2 / H^2 / 0.4e1) * S3 * n - (-v0 / H / 0.2e1 + v2 / H / 0.2e1 + v1 / r1) * T1 * S3 * m / Tref - (-v0 / H / 0.2e1 + v2 / H / 0.2e1 + v1 / r1) * S3 - ((-0.1e1 / H^2 + 0.1e1 / H / r1 / 0.2e1) * T0 + 0.2e1 * T1 / H^2 + (-0.1e1 / H^2 - 0.1e1 / H / r1 / 0.2e1) * T2) * S4;$$

$$F3i = -(((vim1 - vi1) * uim1 / H^2 / 0.4e1 + vi * ui / ri^2 + (-vi1 + vim1) * ui1 / H^2 / 0.4e1) * Ti * S3 * m / Tref + ((vim1 - vi1) * uim1 / H^2 / 0.4e1 + vi * ui / ri^2 + (-vim1 + vi1) * ui1 / H^2 / 0.4e1) * S3 * n - (-vim1 / H / 0.2e1 + vi1 / H / 0.2e1 + vi / ri) * Ti * S3 * m / Tref - (-vim1 / H / 0.2e1 + vi1 / H / 0.2e1 + vi / ri) * S3 - ((-0.1e1 / H^2 + 0.1e1 / H / ri / 0.2e1) * Tim1 + 0.2e1 * Ti / H^2 + (-0.1e1 / H^2 - 0.1e1 / H / ri / 0.2e1) * Ti1) * S4;$$

$$F3N = -(((vnm1 - vn1) * unm1 / H^2 / 0.4e1 + vn * un / rn^2 + (-vnm1 + vn1) * un1 / H^2 / 0.4e1) * Tn * S3 * m / Tref + ((vnm1 - vn1) * unm1 / H^2 / 0.4e1 + vn * un / rn^2 + (-vnm1 + vn1) * un1 / H^2 / 0.4e1) * S3 * n - (-vnm1 / H / 0.2e1 + vn1 / H / 0.2e1 + vn / rn) * Tn * S3 * m / Tref - (-vnm1 / H / 0.2e1 + vn1 / H / 0.2e1 + vn / rn) * S3 - ((-0.1e1 / H^2 + 0.1e1 / H / rn / 0.2e1) * Tnm1 + 0.2e1 * Tn / H^2 + (-0.1e1 / H^2 - 0.1e1 / H / rn / 0.2e1) * Tn1) * S4;$$